3-1-1990

Advances in Nonlinear Matched Filtering

O. K. Ersoy
Purdue University

Y. Yoon
Purdue University

N. Keshava
Purdue University

D. Zimmerman
Purdue University

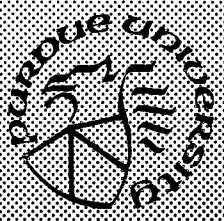

Advances in Nonlinear Matched Filtering

O. K. Ersoy
Y. Yoon
N. Keshava
D. Zimmerman

TR-EE-90-23
March 1990

School of Electrical Engineering
Purdue University
West Lafayette, Indiana 47907

ADVANCES IN NONLINEAR MATCHED FILTERING

O. K. Ersoy, Y. Yoon, N. Keshava, D. Zimmerman

Purdue University
School of Electrical Engineering
W. Lafayette, IN 47907

CONTENTS

ABSTRACT

Symmetric nonlinear matched filters (SNMF's) involve the transformation of the signal spectrum and the filter transfer function through pointwise nonlinearities before they are multiplied in the transform domain. The resulting system is analogous to a 3-layer neural net. The experimental and theoretical results discussed indicate that SNMF's hold considerable potential to achieve high-power of discrimination, resolution and large SNR. The statistical analysis of a particular SNMF in the 2-class problem indicates that the performance coefficient of the SNMF is about four times larger than the performance coefficient of the classical matched filter. In terms of resolving closeby signals, there seems to be no limit to the achievable resolution. However, intermodulation noise has to be carefully monitored.

1. INTRODUCTION

The matched filter was first described by North in 1943[1]. Since the development of the Vander Lugt optical correlator[2], matched filtering has been a major area of research interest in the optics community. The classical matched filter (CMF) is the optimum linear time-invariant (LTI) (or space-invariant, LSI) filter for detecting a known signal in additive, at least wide-sense stationary (WSS) noise which is uncorrelated with the signal. The optimality of the CMF is based on the maximum signal-to-noise ratio (SNR) achievable with the filter based on convolution.

However, the optimum filter for a given application depends strongly on the constraints of the intended application. In pattern recognition, the problem is to classify a signal as belonging to a particular class. In the CMF tuned to a particular class, signals belonging to other classes are considered noise. Since such signals are usually highly correlated with the signal for the particular class, the CMF is not optimal. Often, the problem is to detect a small image, say, a target, in a global image. In this case, the reference image with which the input image is correlated is different from the input image, and the properties of the CMF, such as the centroid of the target being where the correlation peak is, do not necessarily hold. Another problem with the CMF is that targets which are closeby cannot be resolved.

As most other filters, the CMF is based on convolution (correlation). If other types of operations are allowed, the question of what filter is optimal is an open research issue. However, convolution is very powerful since it is easy to implement, shift-invariant and indicates the position of the target at the position of the correlation peak. Any other type of filter to be suggested needs to have similar properties.

In optical signal processing, the generation of complex spatial filters for real-time applications is not trivial. Computer-generated holograms[3] can be used to synthesize filters, but they are not easily adaptable in real-time, and highly accurate positioning is needed. Some of these restrictions can be removed by joint transform correlators[4,5] for which a square-law detector is needed in the focal plane of the optical system. Initially, due to the limitations of the spatial light modulator (SLM) technology, a number of filters related to the CMF were developed. In

phase-only (POF) filters[6], the amplitude of the filter is kept constant while its phase corresponds to the phase of the matched filter. In binary phase-only (BPOF) filters[7], the filter transfer function value at each point is further reduced to 1 when the real (or the imaginary) part of the spectrum is positive, and -1 otherwise. This approach leads to a 2-D mask easy to generate in real-time.

In a recent paper[8], we discussed generalization of such filters to symmetric nonlinear matched filters (SNMF's) such that both the filter transfer function and the input signal spectrum are passed through a nonlinearity before they are multiplied in the spectral domain. The resulting system was shown to be analogous to a 3-layer neural network.

In this paper, we will discuss further studies with nonlinear matched filters. The paper consists of 10 sections. A review of nonlinear matched filters is given in Sec. 2. Experiments in machine vision with SNMF's are described in Sec. 3. Performance of binary symmetric filter, a particular SNMF, in terms of signal-to-noise ratio, is the subject of Sec 4. Detection of a small image, for example, a target, in a global image is discussed in Sec. 5. The topic of resolution, artifacts and intermodulation noise is covered in Sec. 6. The design of SNMF's based on the cosine transforms is the subject of Sec 7. In Sec 8, a statistical analysis of SNMF's is covered. Sec. 9 is a discussion, especially related to optical implementations. Conclusions are reached in Sec 10. In all sections, the results are discussed in comparison to CMF's. Some of the properties of the CMF's which are often overlooked in the literature also become clear in this process.

2. A REVIEW OF NONLINEAR MATCHED FILTERS

The symmetrical nonlinear matched filters considered in this paper have a block diagram as shown in Fig. 1. Both the signal spectrum and the filter transfer function are passed through the nonlinearities N_1 and N_2, respectively, before being multiplied in the spectral domain.

The transform T used in previous experiments discussed in Ref. 8 was either the DFT or the RDFT. It was also shown that the RDFT-based filters are superior in terms of signal discrimination, lack of false correlation signals and artifacts than the corresponding DFT-based filters. For this reason, the RDFT will be the transform mostly used in the following sections. In Sec. 7, the use of cosine transforms for easier optical implementations will be discussed. It is noted that the CMF is the same whether it is implemented by the DFT or the RDFT.

The 2-D RDFT of the first kind is the discretization of the 2-D real Fourier transform of the first kind, which can be written for a signal s(x,y) as[8]

$$S(u,v) = \int_{-\infty}^{\infty}\int_{-\infty}^{\infty} s(x,y)\cos(2\pi ux + \theta(u))\cos(2\pi vy + \theta(v))dxdy \qquad (1)$$

where

$$\theta(f) = \begin{cases} 0 & f \geq 0 \\ \frac{\pi}{2} & f < 0 \end{cases} \tag{2}$$

The inverse transform is

$$s(x,y) = 4\int_{-\infty}^{\infty}\int_{-\infty}^{\infty} S(u,v)\cos(2\pi ux + \theta(u))(\cos 2\pi vy + \theta(v))dudv \tag{3}$$

The corresponding 2-D RDFT for a discrete 2-D sequence $s(n_1,n_2)$ of size $N_1 \times N_2$ is given by[8]

$$S(n_1,n_2) = \sum_{k_1=0}^{N_1-1}\sum_{k_2=0}^{N_2-1} s(k_1,k_2)\cos[\frac{2\pi k_1 n_1}{n_1} + \theta(n_1)]\cos[\frac{2\pi k_2 n_2}{N_2} + \theta(n_2)] \tag{4}$$

with the inverse transform

$$s(n_1,n_2) = \frac{4}{N_1 N_2}\sum_{k_1=0}^{N_1-1}\sum_{k_2=0}^{N_2-1} S(k_1,k_2)v(k_1)v(k_2)\cos[\frac{2\pi k_1 n_1}{N_1} + \theta(k_1)]\cos[\frac{2\pi n_2 k_2}{N_2} + \theta(k_2)] \tag{5}$$

where

$$\theta(n) = \begin{cases} 0 & 0 \leq n \leq N/2 \\ \frac{\pi}{2} & n > N/2 \end{cases} \tag{6}$$

and

$$v(n) = \begin{cases} 1 & n \neq 0, N/2 \\ 1/2 & \text{otherwise} \end{cases} \tag{7}$$

The four quadrants of the 2-D real Fourier spectral plane involves 4 types of sine-cosine operations shown in Fig. 2.

The relationship between the 2-D DFT and the 2-D RDFT coefficients can be written as follows:

$$F(n_1,n_2) = S_1(n_1,n_2) - j\,S_0(n_1,n_2) \tag{8}$$

where $F(n_1,n_2)$ is the DFT coefficient, $S_1(n_1,n_2)$ and $S_0(n_1,n_2)$ in terms of $S(n_1,n_2)$ are described in Table 1.

The fast computation of 2-D linear and circular convolution (correlation) by the 2-D RDFT is discussed in Ref.8. The computations involved are outlined in the Appendix.

Use of RDFT leads to the definitions of the RDFT-based POF, and BPOF filters[8]. The final system is still linear since no nonlinearity is applied to the signal spectrum, and the system implements convolution.

The 2-D RDFT spectral coefficients are real when the input signal is real. Consequently, amplitude and phase are defined differently from the way they are defined with the 2-D DFT. The definition of the amplitude $R(n_1,n_2)$ connects the 4 RDFT coefficients $S(n_1,n_2), S(N_1-n_1,N_2-n_2), S(N_1-n_1,n_2), S(n_1,N_2-n_2)$ and is shown in Table 2.

The RDFT-based POF is obtained by normalizing the four related spectral values referred to above by $R(n_1,n_2)$. The RDFT-based BPOF is obtained by hard-limiting each individual spectral value to $\pm a_0$ where a_0 is a constant number. If a_0 is 1, the nonlinearity is the bipolar hard-limiter:

$$S'(n_1,n_2) = \text{sgn}[S(n_1,n_2)] = \begin{cases} 1 & S(n_1,n_2) \geq 0 \\ -1 & \text{otherwise} \end{cases} \tag{9}$$

The corresponding symmetric nonlinear matched filters are obtained by applying the operations described above to the RDFT spectra of both the signal and the filter. The resulting filters are called symmetric POF (SPOF) and the symmetric binary filter (SBF), respectively.

Experimentally, the RDFT-based SBF was found to be the best in terms of discrimination ability among all NMF's[8]. In the next section, its performance in machine vision is further discussed.

3. EXPERIMENTS IN MACHINE VISION

We studied the performance of the RDFT-based SBF in machine vision in comparison to the CMF. The particular problem in machine vision we investigated is parts classification and inspection during the machining of parts. We were to classify the tools in the Cincinnati Milacron T10 tool chain in the Machine Vision Laboratory of Purdue University shown in Fig. 3, and to inspect whether they are broken or not after *correct* classification.

There were thirty different tools located on the tool chain. In our initial experiments, we utilized 8 of these and a broken tool, shown in Figs. 4 and 5.

In this type of problem, there are as many matched filters as the number of classes N, but only the correlation peak at the center of the correlation plane for each filter is of interest. The procedure for the implementation of the ith SBF tuned to a particular class i is as follows:

1. The 2-D RDFT of the reference image representing class i is computed. The result is passed thru the nonlinearity given by Eq. (9). Let the final result be denoted by $H_i(n_1,n_2)$.
2. The 2-D RDFT of the input image $s(n_1,n_2)$ is computed, and the result is passed through the nonlinearity given by Eq. (9). Let the final result be denoted by $S'(n_1,n_2)$.
3. Using Eqs. (A.1) through (A.7) in the Appendix for the computation of convolution, it can be shown that the output of the ith filter is given by

$$z(i) = \frac{1}{N_1 N_2} \sum_{k_1=0}^{N_1-1} \sum_{k_2=0}^{N_2-1} H_i'(k_1,k_2) S'(k_1,k_2) \tag{10}$$

If 2-D linear cross-correlation rather than 2-D circular cross-correlation is desired $x(n_1,n_2)$ and $h(n_1,n_2)$ are zero-padded to size $2N_1 \times 2N_2$, and the transform size is doubled in both directions. This is what is done in all experiments discussed in the succeeding sections, except for those involving cosine transforms.

Fig. 6 shows the binary image obtained by thresholding of the 2-D RDFT spectrum of tool no. 7. It is observed that the resulting SBF system is basically a 3-layer neural network, as shown in Fig. 7. The first stage is the transform. This is followed by the pointwise nonlinearities. The second stage W has elements $w_{ik_1k_2}$ given by

$$w_{ik_1k_2} = \frac{1}{N_1 N_2} H_i'(k_1,k_2) \tag{11}$$

Since there are 8 classes, there are 8 output neurons. The class is decided by a winner-take-all network whose input is the output of the NMF-based network. After the classification, the part is inspected as to whether it is satisfactory. This is, for the time being, done by comparing the output of the NMF-based network for the particular class with the expected output in terms of a threshold value.

In the experiments, the initial images were of size 256×256. They were reduced to size 64×64 by averaging over 16×16 blocks in order to reduce variations in the lighting conditions and to achieve higher speed of processing. The images were obtained with a camera located over the T10 machine tool chain, whose output was digitized by an ITEX 150 real-time image processing system and sent to a SUN workstation for further processing.

The 2-D SBF-based system was studied in comparison to the 2-D CMF-based system. Tables 3 and 4 show the corresponding results. Each item was normalized by the largest item per row. It is observed that the CMF-based system was very poor in terms of classification. The SBF-based system was excellent, giving no classification error as well as showing a very high power of discrimination.

Table 5 shows how the inspection of Tool No. 7 is carried out after being chosen as the correct class. We see here why it is important to have high power of discrimination. It makes possible to classify correctly, even though the tool is broken, since the correlation peak value is considerably lower than the peak value with the nonbroken tool.

An important consideration in such experiments is the lighting conditions. In many other techniques, it is necessary to segment the image. When the lighting conditions change, the segmentation results also tend to change. The NMF-based network does not need segmentation. In addition, the light intensity level is immaterial due to the threshold nonlinearity after the spectral transformation. We can also compensate for the changing lighting conditions by having more than 1 output value per class corresponding to different sample lighting conditions, or by

learning the weights optimally under such conditions.

It is observed in Table 3 that the CMF-based network is always choosing class 1. This is expected to be due to the higher overall brightness of the class 1 image. The same type of result is obtained even if class 1 is discarded and the experiments are repeated with 7 classes. It is possible to normalize the image brightness levels, but this is expected to be not very reliable, especially under changing lighting conditions. The NMF-based network gets around such problems due to the threshold nonlinearity.

4. PERFORMANCE OF BINARY SYMMETRIC FILTER IN TERMS OF SIGNAL-TO-NOISE RATIO

The CMF is optimal in terms of maximum SNR achievable with a LTI or LSI system for detecting a signal in additive, WSS noise uncorrelated with the signal. The total input signal to the filter can be written as

$$s(x) = f_i(x) + n_i(x) \tag{12}$$

where $f_i(x)$ is the signal of interest and $n_i(x)$ is noise. The output of the filter is

$$y(x_1) = fo(x) + n_0(x) \tag{13}$$

SNR_1, the signal-to-noise ratio for the CMF, is commonly defined as

$$SNR_1 = \frac{f_0^2(x_0)}{E[n_0^2(x)} \tag{14}$$

where x_0 is the time of measurement at which SNR_1 is maximum. However, in connection with optical matched filters, SNR_1 has been equivalently defined as[7]

$$SNR_1' = \frac{|f_0(x_0)|}{[E[n_0^2(x)]]^{1/2}} \tag{15}$$

This is the definition which is used in most of the experiments to be described.

In image detection by various matched filters, other definitions of SNR have been developed. One such definition, to be referred to as SNR_2, also known as the Horner efficiency, is given by[7]

$$SNR_2 = k \sum_{A'} |R(x)|^2 / \sum_{A} |R(x)|^2$$

$$= kE_A'/E_A \tag{16}$$

where R(x) represents the value at point x on the correlation plane, k is a constant representing the fraction of light that gets through the correlation filter, E_A and E_A' are the energies in the total output plane A and the region A′ corresponding to the half-power (intensity) region of the correlation peak. k was chosen as 1 in the experiments.

One problem in the definition of SNR_1' given by[7] Eq. (15) is how to estimate the mean square error in practical experiments. One possible way is to assume that it is given by

$$E[n_0^2(x)] \sim \frac{1}{N_A - N'_A} \sum_{A-A'} | R(x_i) |^2 \tag{17}$$

where N_A is the total number of pixels, and N'_A is the number of pixels under the 50% response portion of the correlation peak. Then, SNR_1' can be written as

$$SNR_1' = \left[\frac{N_A [R(x_i)]^2_{max}}{(1 - SNR_2) \sum_{A} | R(x_i) |^2} \right] \tag{18}$$

One disadvantage of SNR_1' as defined above is that it is possible to get isolated regions away from the central correlation peak which give values greater than $[R(x)]_{max}/\sqrt{2}$. In order to prevent that these regions are also considered as belonging to the signal, we modifed the definition of SNR_1' as follows:

The regions with values above $[R(x)]_{max}/\sqrt{2}$ are quantized as 1 and all other regions are quantized as zero. Then, the "1" region and the "0" region are considered as the signal part and the noise part, respectively. $E[n_0^2(t)]$ is still estimated by Eq. (17), with N_A and N_A' determined from the two regions.

Based on the SNR measures described above, we studied the comparative performance of the CMF and the SBF with the Purdue campus image shown in Fig. 8. This image was corrupted by white Gaussian noise with standard deviation equal to 10, 20, 30, 40, 50, 60 and 70. Figs. 9 and 10 show the corrupted images with white noise standard deviation equal to 10 and 70, respectively.

Table 6 shows the comparative performance of the CMF and the SBF as a function of SNR_1' without modification. Table 7 shows the same type of results when the modified SNR_1' with the SBF filter is used. Considerably larger SNR_1' with the SBF filter is observed even in very large noise.

5. DETECTION OF A SMALL IMAGE IN A GLOBAL IMAGE

In many applications, the problem is the detection of a small image, such as a target or a medical anomally, in a global image. It is often assumed that the CMF gives the correct location of the small image in the global image. This is not necessarily true, especially as the dimensions of the small image gets smaller. The experiments discussed below shows that the SBF gives more accurate results than the CMF in this problem.

The global image was chosen as the Purdue campus image of Fig. 8. The small image was generated by choosing 4 different window locations as shown in Fig. 11. Both rectangular and Hanning windows were used. The windowed image was used as the reference image, to be correlated with the global image in additive white Gaussian noise. Different window sizes were

chosen, starting with a size of 64 × 64. The correct location of the correlation peak is the center of the correlation plane. The distance of the correlation peak from the center shows the amount of error.

Tables 8 thru 11 show the average results with the rectangular window as a function of window size and standard deviation of additive white noise. Tables 12 thru 15 are the corresponding results with the Hanning window. Averaging was done over the results of the four windows shown in Fig. 11. Tables 8 and 12 show the average distance of the correlation peak from the center of the correlation plane with the CMF system. Tables 9 and 13 show the corresponding results with the SBF system. Both systems make errors as the window size gets smaller, but the SBF system is considerably better than the CMF system at all noise levels. Tables 10 and 14 show the average modified SNR_1' with the CMF system. Tables 11 and 15 show the corresponding results with the SBF system. The SBF system is considerably better than the CMF system at all window sizes and noise levels. One conclusion for both systems is that reasonably large SNR does not necessarily mean that the correlation peak is at the right position.

The experiments discussed above were repeated with images which were edge-enhanced by the Sobel operator. The results were worse than the results without edge-enhancement. These preliminary results indicate that edge-enhancement is not necessarily useful for correct positioning of the correlation peak or increased SNR.

Another important problem is to detect motion by correlation. The relative movement of the correlation peak of the CMF system shows exactly how much an object moved in the x and y directions. The SBF system is not linear, and the question is whether it still has this property. To answer this question, we generated a 20 × 20 window at the center of the Purdue campus image and moved it to the four corners of the image plane. Table 16 shows how much the actual window and the correlation peak moved in the x and y directions as a function of standard deviation of additive, white noise. It is observed that the two movements match exactly except at very large noise levels.

6. RESOLUTION, ARTIFACTS AND INTERMODULATION NOISE

By resolution, we mean the ability to resolve signals which are very close to each other. By artifacts and intermodulation noise, we mean false correlation peaks which may be identified as signal. Artifacts and intermodulation noise may also cause concealing of actual signals. In this section, we will discuss these issues with respect to the RDFT- and the DFT-based NMF's.

First, we consider the increase of noise when a small image is correlated with a global image as in Sec. 5. Fig. 12 shows the output of the RDFT-based SBF when the Purdue image of Fig. 8 is correlated with itself in additive noise with $\sigma = 10$. Fig. 13 shows the corresponding result with the DFT-based SBF. Figs. 14 and 15 are the same type of results except that the reference image is a 32 × 32 central block of the Purdue image. It is clear that the RDFT-based SBF is much better than the DFT-based SBF in terms of noise.

Next, we will discuss two experiments to understand intermodulation noise. In the first experiment, a letter E was repeated four times to generate an image of size 32 × 32, and then the image was zero-padded to size 64 × 64. The filter was designed for one letter E. Fig. 16 shows the four correlation peaks obtained with the RDFT-based SPOF. The correlation peaks are of equal height. Fig. 17 shows the corresponding result with the DFT-based SPOF. The correlation peaks are unequal and there are other peaks in the form of intermodulation noise.

The third experiment was similar to the second experiment except that 2 letters were changed to F. Fig. 18 shows the four correlation peaks obtained with the RDFT-based SPOF. The two large peaks correspond to letter E, and the two smaller peaks correspond to letter F. The filter is very sensitive to the difference between letters E and F. Fig. 19 shows the corresponding result with the DFT-based SPOF. It is impossible to differentiate between the two letters and there is more intermodulation noise.

When two signals are in close proximity, CMF's cannot resolve the two signals, and a single correlation peak is obtained. We studied the corresponding performance of SPOF. Figure 20 shows the output of the RDFT-based SPOF when two letters E are detected. Figure 21 is the corresponding output of the DFT-based SPOF with intermodulation peaks. Figures 22 and 23 show what happens with both filters when the two E's overlap and the hidden part of the underlying E is removed.

No matter how close the two signals are, the SPOF is capable of resolving them. If the hidden part is not removed, but the two signals are simply added, the outputs become as in Figs. 24 and 25. Again, the DFT-based filter results in intermodulation peaks.

7. NONLINEAR MATCHED FILTERS BASED ON COSINE TRANSFORMS

The results in the previous sections have shown that the RDFT-based NMF's have superior performance. Digital implementation of the RDFT is considerably simpler than the digital implementation of the DFT. On the other hand, the DFT can be considered to be the approximation of the complex Fourier transform, which is straightforward to implement using coherent light and a Fourier lens. The RDFT can be considered to be the approximation of the real Fourier transform, which is not as simple to implement optically.

It is desirable to have the spectral coefficients real except for sign since the pointwise nonlinear operations can be more easily achieved optically. One way to achieve this result is by making the input image symmetric, which reduces the complex Fourier transform to a cosine transform.

There are two possible symmetries resulting in two types of cosine transforms. Consider Fig. 26 with 4-fold symmetry. This leads to the reduction of the complex Fourier transform to the cosine transform of the first kind. If two images at opposite corners are skipped, 2-fold symmetry is obtained, and the complex Fourier transform reduces to the cosine transform of the second kind.

In the discrete domain, the 4-fold symmetry means, for $0<n_1<N_1/2$ and $0<n_2<N_2/2$,

$$s(n_1,n_2) = s(N_1-n_1,n_2) = s(n_1,N_2-n_2) = s(N_1-n_1,N_2-n_2) \tag{19}$$

where N_1,N_2 are the two dimensions of the image. With 4-fold symmetry, the 2-D DFT reduces to the 2-D discrete symmetric cosine transform of the first kind (DSCT1):

$$S(n_1,n_2) = \sum_{k_1=0}^{N_1-1}\sum_{k_2=0}^{N_2-1} s(k_1,k_2)\cos\frac{2\pi n_1 k_1}{N_1}\cos\frac{2\pi n_2 k_2}{N_2} \tag{20}$$

$S(n_1,n_2)$ is also 4-fold symmetric.

The 2-fold symmetry corresponds to

$$s(n_1,n_2) = s(N_1-n_1,N_2-n_2) \tag{21}$$

for $0<n_1<N_1/2, 0<n_2<N_2$. With 2-fold symmetry, the 2-D DFT reduces to the 2-D DSCT of the second kind (DSCT2):

$$S(n_1,n_2) = \sum_{k_1=0}^{N_1-1}\sum_{k_2=0}^{N_2-1} s(k_1,k_2)\cos 2\pi\left[\frac{n_1 k_1}{N_1}+\frac{n_2 k_2}{N_2}\right] \tag{22}$$

$S(n_1,n_2)$ is also 2-fold symmetric.

The DSCT-based SBF is constructed the same way as the RDFT-based SBF. Figure 27 shows the output of the DSCT1-based SBF when the Purdue image of Fig. 8 was correlated with itself after adding white noise with $\sigma = 10$. Figure 28 shows the corresponding result when the reference image was the 32×32 central block of the Purdue image.

The image of Fig. 26 was correlated with itself using the DFT-based SBF. Because of 4-fold symmetry, this is the same as the DSCT2-based SBF. The result is shown in Fig. 29. The correlation peaks at the edges are believed to be due to the circular nature of correlation since no zero-padding was utilized.

We also repeated the experiments regarding SNR_1' and detection of a small image in a global image with the DSCT1. Tables 17 and 18 show the average distance of the correlation peak from the center of the correlation plane with the DSCT1-based CMF and SBF. Tables 19 and 20 show the average modified SNR_1' with both systems. As before, we conclude that the SBF system is considerably better than the CMF system at all window sizes and noise levels.

In conclusion, NMF's constructed with cosine transforms may be easier to implement optically and give good performance. However, we expect to get intermodulation noise problems since they are actually a constrained version of NMF's based on the complex Fourier transform.

8. ANALYSES OF NONLINER MATCHED FILTERS

Binary filters for pattern classification have recently been statistically analyzed for the two-class problem in which the input signals were assumed to be stationary and white[9]. In this section, we will extend this analysis to symmetric binary filters. For the sake of simplicity, 1-D

analysis will be presented.

In the two-class problem, the filter will be assumed to be designed for Class 1. The performance measure can be chosen as the performance coefficient ρ defined by[9]

$$\rho = \frac{(\mu_1 - \mu_2)^2}{\eta_1 + \eta_2} \tag{23}$$

where, for n = 1 or 2,

$$\mu_n = \sup_x [E[R_n(x)]]$$

$$\eta_n = \sup_x [VAR[R_n(x)]] \tag{24}$$

$R_A(x)$ is the correlation output for Class n, and VAR $[R_n(x)]$ denotes variance of $R_n(x)$. In Eq. (23), the term in the numerator measures the relative size of the correlation peaks for the two classes, whereas the term in the denominator indicates the average energy in the sidelobes. Consequently, ρ is a measure of how well the filter discriminates Class 1 from Class 2. When the output $R_n(x)$ is Gaussian, and the *a priori* probabilities of the two classes are the same, ρ is identical with the Bhattacharyya coefficient[10].

In the linear case, the analysis of ρ for statistically uncorrelated pattern classes indicates that the binary filters provide classification performance comparable to, but bounded above by the CMF. In comparison, the SBF will be shown to be superior to the CMF in terms of ρ.

The signals $s_1(x)$ for Class 1 and $s_2(x)$, for Class 2, will be assumed to be sample realizations of independent, zero mean, stationary, white random processes with variances equal to σ_1^2 and σ_2^2, respectively.

The 1-D real Fourier transform of $s_n(x)$ can be written as a pair of equations given by[11]

$$S_{1n}(f) = \int_{-\infty}^{\infty} s_n(x)\cos 2\pi fx \, dx \tag{26a}$$

$$S_{0n}(f) = \int_{-\infty}^{\infty} s_n(x)\sin 2\pi fx \, dx \tag{26b}$$

with the inverse transform

$$s_n(x) = \int_0^{\infty} \left[S_{1n}(f)\cos 2\pi fx + S_{0n}(f)\sin 2\pi fx \right] df \tag{27}$$

$s_1(x)$ and $s_2(x)$ will be limited to a window such that $|x| \le W_x$. We will also assume that $S_n(f)$ is known for $|f| \le W_f$. Then, Eqs. (26) and (27) can be written as

$$S_{1n}(f) = \int_{-W_x}^{W_x} s_n(x)\cos 2\pi fx \, fx \tag{28a}$$

$$S_{0n}(f) = \int_{-W_x}^{W_x} s_n(x)\sin 2\pi fx \, dx \tag{28b}$$

$$s_n(x) = 2\int_0^{W_f} \left[S_{1n}(f)\cos 2\pi fx + S_{0n}(f)\sin 2\pi fx\right] df \tag{29}$$

Since $s_n(x)$ for n equal to 1 and 2 are independent and zero mean, $S_{11}(f), S_{12}(f), S_{01}(f), S_{02}(f)$ can be assumed to be independent, zero mean, Gaussian random processes according to central limit theorem. Then, the following statistics can be written:

$$E\left[S_{1n}(f)\, S_{0n}(f)\right] = 0 \tag{30}$$

$$E\left[S_{1n}(f_1)S_{1n}(f_2)\right] = \sigma_n^2 W_x \left[\text{sinc}2W_x(f_1 - f_2) + \text{sinc}2W_x(f_1 + f_2)\right] \tag{31}$$

$$E\left[S_{0n}(f_1)S_{0n}(f_2)\right] = \sigma_n^2 W_x \left[\text{sinc}2W_x(f_1 - f_2) - \text{sinc}2W_x(f_1 + f_2)\right] \tag{32}$$

$$E\left[\text{sgn}(S_{1n}(f))\right] = 0 \tag{33}$$

$$E\left[|S_{1n}(f)|\right] = \frac{\sqrt{2W_x\sigma_n^2}}{\sqrt{\pi}} \sqrt{1 + \text{sinc}4W_x f} \tag{34}$$

$$E\left[\text{sgn}(S_{1n}(f_1))\text{sgn}(S_{1n}(f_2))\right] = \frac{2}{\pi}\sin^{-1} r_1(f_1, f_2) \tag{35}$$

$$E\left[|S_{1n}(f_1)|\ |S_{1n}(f_2)|\right] = \frac{2W_x\sigma_n^2}{\pi} \left[(1 + \text{sinc}4W_x f_1)^{\frac{1}{2}} (1 + \text{sinc}4W_x f_2)^{\frac{1}{2}} (1 - r_1^2(f_1, f_2))^{\frac{1}{2}} + (\text{sinc}2W_x(f_1 - f_2) + (\text{sinc}2W_x(f_1 + f_2))\sin^{-1} r_1\ (f_1, f_2)\right] \tag{36}$$

where $r_1(f_1, f_2)$ is the correlation coefficient between $S_{1n}(f_1)$ and $S_{1n}(f_2)$, given by

$$r_1(f_1, f_2) = \frac{\text{sinc}2W_x(f_1 - f_2) + \text{sinc}2W_x(f_1 + f_2)}{(1 + \text{sinc}4W_x f_1)^{\frac{1}{2}} (1 + \text{sinc}4W_x f_2)^{\frac{1}{2}}} \tag{37}$$

We will also need the correlation coefficient $r_0(f_1, f_2)$ between $S_{0n}(f_1)$ and $S_{0n}(f_2)$. It is given by

$$r_0(f_1,f_2)=\frac{\text{sinc}2W_x(f_1-f_2)-\text{sinc}2W_x(f_1+f_2)}{(1-\text{sinc}4W_xf_1)^{\frac{1}{2}}(1-\text{sinc}4W_xf_2)^{\frac{1}{2}}} \tag{38}$$

In the case of the CMF, the correlation outputs are given by

$$R_1(x)=2\int_0^{W_f}\left[S_{11}^2(f)+S_{01}^2(f)\right]\cos 2\pi fx\,dx \tag{39}$$

$$R_2(x)=2\int_0^{W_f}\left[S_{11}(f)S_{12}(f)+S_{01}(f)S_{02}(f)\right]\cos 2\pi fx\,dx+2\int_0^{W_f}\left[S_{01}(f)S_{12}(f)-S_{11}(f)S_{02}(f)\right]\sin 2\pi fx\,dx \tag{40}$$

The means and the variances are[9]

$$\mu_1=\rho\sigma_1^2 \tag{41}$$

$$\mu_2=0 \tag{42}$$

$$\eta_1=4p^2\sigma_1^2\alpha(p) \tag{43}$$

$$\eta_2=2p^2\sigma_1^2\sigma_2^2\alpha(p) \tag{44}$$

where p is the space-bandwidth product equal to $4W_xW_f$, and

$$\alpha(p)=\int_0^1(1-u)(\text{sinc}pu)^2\,du \tag{45}$$

The performance coefficient ρ^M for the CMF becomes

$$\rho^M=\frac{\sigma^2}{2\alpha(p)(1+2\sigma^2)} \tag{46}$$

where σ^2, called the class spread ratio, equals σ_1^2/σ_2^2.

Let $\text{sgn}(S_{mn}(f))$ be denoted by $S'_{mn}(f)$. Then, the correlation outputs of the SBF can be written as

$$R_1(x)=2\int_0^{W_f}\left[S'^2_{11}(f)+S'^2_{01}(f)\right]\cos 2\pi fx\,df \tag{47}$$

$$R_2(x)=2\int_0^{W_f}\left[S'_{11}(f)S'_{12}(f)+S'_{01}(f)S'_{02}(f)\right]\cos 2\pi fx\,df+2\int_0^{W_f}\left[S'_{01}(f)S'_{12}(f)-S'_{11}(f)S'_{02}(f)\right]\sin 2\pi fx\,df \tag{48}$$

It can be shown that the means and the variances are given by

$$\mu_1 = 4W_f \tag{49}$$

$$\mu_2 = 0 \tag{50}$$

$$\eta_1 = 0 \tag{51}$$

$$\eta_2 = \sup_x \mathrm{VAR}\left[R_2(x)\right] \tag{52}$$

where

$$\mathrm{VAR}\left[R_2(x)\right] = \frac{16}{\pi^2}\int_0^{W_f}\int_0^{W_f}\left[\left[\sin^{-1}r_1(f_1,f_2)\right]^2 + \left[\sin^{-1}r_0(f_1,f_2)\right]^2\right]\cos 2\pi f_1 x \cos 2\pi f_2 x\, df_1\, df_2$$

$$+\frac{32}{\pi^2}\int_0^{W_f}\int_0^{W_f}\sin^{-1}r_1(f_1,f_2)\sin^{-1}r_0(f_1,f_2)\sin 2\pi f_1 x \sin 2\pi f_2 x\, df_1\, df_2 \tag{53}$$

The performance coefficient ρ for the SBF becomes

$$\rho^S = \frac{16W_f^2}{\eta_2} \tag{54}$$

where η_2 needs to be evaluated numerically from Eqs. (52) and (53).

An interesting observation is that ρ^S does not depend on σ_1^2 and σ_2^2. On the other hand, ρ^S depends on W_x and W_f separately rather on than their product.

Table 21 shows the performance coefficients ρ^M and ρ^S as a function of the class spread ratio σ^2 and the window sizes W_x and W_f. It is observed that ρ^S is almost four times larger than ρ^M.

9. DISCUSSION

Above we discussed a number of techniques for symmetric nonlinear matched filtering. A major question is how to implement such techniques optically.

The 2-D RDFT can be implemented by a number of techniques used in digital optics[12,13,14]. Such techniques may be especially well-suited for coupling light into arrays of nonlinear optical devices as discussed subsequently.

The nonlinear operations discussed in the previous sections can be achieved by a number of electro-optical and all-optical techniques. Nonlinear filters such as POF and BPOF were initially developed because of ease of implementation with optical devices such as spatial light modulators.

Perhaps the simplest approach for the real-time nonlinear control of the signal spectrum is the video or the photodiode array registration of the signal spectrum which is modulated by a coherent reference wave, nonlinear modulation of the resulting signal by analog electronics, writing of the transformed signal to a spatial light modulator, and further optical processing.

This is why cosine transform implementations may be especially easy.

A number of integrated optical devices hold great promise for the same purpose. Two such technologies are the arrays of Fabry-Perot etalons containing semiconductor nonlinear refractive materials [15], and the quantum well self-electro-optic devices (SEED) [16]. The first technology requires high input optical power at the moment. The SEED's, on the other hand, require very little switching energy.

Certain types of spatial light modulators can also be used for nonlinear processing. One example is the microchannel spatial light modulator, which is capable of analog thresholding and real-time hard-clipping [17].

In this paper, only the hard-limiting nonlinearity is considered. This can be replaced by other types of nonlinearities. The biopolar threshold function corresponds to a very high degree of discrimination. It is possible to choose the nonlinearity adaptively, as shown in Fig. 30. When the nonlinearity gets steeper than linear as in (A), the discrimination power of the network increases. The linear case(B) corresponds to the CMF. When the nonlinearity has slope which is less than linear as in (C), the discrimination power of the filtering system decrease further, and, more and more, patterns which have some resemblance are characterized as belonging to the same class.

10. CONCLUSIONS

The experimental and theoretical results discussed indicate that symmetric nonlinear matched filters hold considerable potential to achieve high power of discrimination, resolution, and large SNR. They are analogous to 3-layer neural networks.

The statistical analysis in terms of the 2-class problem indicates that the perform once coefficient of the SBF is about four times larger than the performance coefficient of the CMF. This is in agreement with all the experimental evidence. Similar analysis is needed for the M-class problem, other SNMF's and nonlinearities other than the hard-limiter.

The resolution properties of the SNMF's are highly intriguing. There seems to be no limit to the achievable resolution. However, intermodulation noise needs to be carefully monitored in order not to misinterpret false correlation peaks. In this sense, the RDFT-based filters give the best results.

Symmetric nonlinear matched filters can be further developed by incorporating generalized matched filtering techniques in order to achieve minimum intraclass and maximum interclass separations. Their analogy to neural nets should be further studied to arrive at more optimal and adaptive structures.

The nonlinear operations involved in these new filters can be achieved by a number of electro-optical and all-optical devices such as the microchannel spatial light modulation, Fabry-Perot etalons and the quantum well self-electro-optic devices.

APPENDIX

FAST COMPUTATION OF 2-D CIRCULAR CORRELATION BY 2-D RDFT

We will discuss circular correlation of 2-D sequences $x(n_1,n_2)$ and $h^i(n_1,n_2)$, giving $y^i(n_1,n_2)$, in terms of the 2-D RDFT. Let the 2-D RDFT's of $x(\cdot,\cdot)$, $h^i(\cdot,\cdot)$ and $y^i(\cdot,\cdot)$ be denoted by $X(\cdot,\cdot)$, $H^i(\cdot,\cdot)$ and $Y^i(\cdot,\cdot)$,respectively. In terms of the 2-D circular correlation theorem with the 2-D RDFT, it can be shown the $Y^i(\text{cdot},\cdot)$ can be written as

$$Y^i(0,0) = X_1(0,0)H_0^i(0,0) \tag{A.1}$$

$$Y^i(N_1/2,N_2/2) = X_1(n_1/2,N_2/2)H_1^i(n_1/2,N_2/2) \tag{A.2}$$

When $0<n_1 = 0,N_1/2$, and $0<n_2<N_2/2$,

$$2\begin{bmatrix} Y^i(n_1,n_2) \\ Y^i(n_1,N_2-n_2) \end{bmatrix} = \begin{bmatrix} H^i(n_1,n_2) & H^i(N_1,n_1-n_2) \\ H^i(N_1,-n_2) & -H^i(n_1,n_2) \end{bmatrix} \begin{bmatrix} X(n_1,n_2) \\ X(n_1,N_2-n_2) \end{bmatrix} \tag{A.3}$$

When $0<n_1 MN_1/2, n_2 = 0,N_2/2$,

$$2\begin{bmatrix} Y^i(n_1,n_2) \\ Y^i(N_1,n_2) \end{bmatrix} = \begin{bmatrix} H^i(n_1,n_2) & H^i(N_1-n_1,n_2) \\ H^i(N_1-n_1,n_2) & -H^i(n_1,n_2) \end{bmatrix} \begin{bmatrix} X(n_1,n_2) \\ X(N_1-n_1,n_2) \end{bmatrix} \tag{A.4}$$

Otherwise,

$$\begin{bmatrix} Y^i(n_1,n_2) \\ Y^i(N_1-n_1,n_2) \\ Y^i(n_1,N_2-n_2) \\ Y^i(N_1-n_1,N_2-n_2) \end{bmatrix} = \begin{bmatrix} 1 & 0 & 1 & 0 \\ 0 & 1 & 0 & 1 \\ 0 & 1 & 0 & -1 \\ -1 & 0 & 1 & 0 \end{bmatrix} \begin{bmatrix} Y_1^i(n_1,n_2) \\ Y_0^i(n_1,n_2) \\ Y_1^i(N_1-n_1,n_2) \\ Y_0^i(N_1-n_1,n_2) \end{bmatrix} \tag{A.5}$$

where

$$4\begin{bmatrix} Y_1^i(n_1,n_2) \\ Y_0^i(n_1,n_2) \end{bmatrix} = \begin{bmatrix} H_1^i(n_1,n_2 & (H_0^i(n_1,n_2) \\ H_0^i(n_1,n_2) & -\text{Hsuh1}^i(n_1,n_2) \end{bmatrix} \begin{bmatrix} X_1(n_1,n_2) \\ X_0(n_1,n_2) \end{bmatrix} \tag{A.6}$$

and

$$4\begin{bmatrix} Y_1^i(N_1-n_1,n_2) \\ Y_0^i(N_1-1,n_2) \end{bmatrix} = \begin{bmatrix} H_1^i(N_1-n_1,n_2) & H_0^i(N_1-n_1,n_2) \\ H_0^i(N_1-n_1,n_2) & -H_1^i(N_1-n_1,n_2) \end{bmatrix} \begin{bmatrix} X_1(N_1-n_1,n_2) \\ X_0(N_1-1,n_2) \end{bmatrix} \tag{A.7}$$

Let $S_1(n_1,n_2)$, $S_0(n_1,n_2)$, $S(n_1,n_2)$ denote either $X_1(n_1,n_2)$, $X_0(n_1,n_2)$, $X(n_1,n_2)$, respectively, or $H_1^i(n_1,n_2)$, $H_0^i(n_1,n_2)$, $H^1(n_1,n_2)$, respectively. The relationship between $S_1(n_1,n_2)$, $S_0(n_1,n_2)$, and $S(n_1,n_2)$ is shown in Table 4.3.1.

REFERENCES

1. D. O. North, "Analysis of the Factors which Determine Signal/Noise Discrimination in Rader," *RCA Tech. Rep. PTR-6-C, June 1943*, reprinted in *Proc. IRE*, Vol. 51, 1016-1028, July 1963.

2. A. Vander Lugt, "Signal Detection by Complex Spatial Filtering," *IEEE Tran. Information Theory*, Vol. IT-10, 139, 1964.

3. D. Casasent, "Computer Generated Holograms in Pattern Recognition: A Review," *Optical Engineering*, Vol. 24, No. 5, 724, September/October 1985.

4. C. S. Weaver, J. W. Goodman, "A Technique for Optically Convolving Two Functions," *Applied Optics*, Vol. 5, No. 7, 1248-1249, July 1966.

5. B. Javidi, "Comparison of Binary Joint Transform Correlators and Phase-Only Matched Filter Correlators," *Optical Engineering*, Vol. 28, No. 3, 267-272, March 1989.

6. J. L. Horner, P. D. Gianino, "Phase-Only Matched Filtering, *Applied Optics*, Vol. 23, No. 6, 812, 1984.

7. J. L. Horner, H. O. Bartlet, "Two-Bit Correlation," *Applied Optics*, Vo. 24, No. 18, 2889-2893, 15 September 1985.

8. O. K. Ersoy, M. Zeng, "Nonlinear Matched Filtering," *J. Optical Society of America A*, Vol. 6, No. 6, 835-843, June 1989.

9. S. S. Venkatesh, D. Psaltis, "Binary Filters for Pattern Classification," *IEEE Tran. Acoustics, Speech, Signal Proc.*, Vol. 37, No. 4, 604-611, April 1989.

10. T. Kailath, "The Divergence and the Bhattacharyya Distance Measure in Signal Selection," *IEEE Trans. Commun. Technol.* Vol. COM-15, 52-60, 1967.

11. O. K. Ersoy, "Real Discrete Fourier Transform," *IEEE Tran. Acoustics, Speech, Signal Processing*, Vol. ASSP-33, No. 4, 880-882, August 1985.

12. O. K. Ersoy, "Electro-Optical Processing of Signal Transforms," *Applied Optics*, Vol. 26, 676-681, 15 February 1987.

13. J. W. Goodman, A. R. Dias, L. M. Woody, "Fully Parallel, High-Speed, Incoherent Optical Method for Performing Discrete Fourier Transforms, *Optics Letters*, Vol. 2, 1-3, 1978.

14. I. Glaser, "Noncoherent Parallel Optical Processor for Discrete Two-Dimensional Linear Transformation," *Optics Letters*, Vol. 5, 449-451, 1980.

15. H. M. Gibbs, *Optical Bistability, Controlling Light with Light*, Academic Press, New York, 1985.

16. D. A. B. Miller et al, "The Quantum Well Self-Electro-optic Effect Device: Optoelectronic Bistability and Oscillation, and Self-Linearized Modulation," *IEEE J. Quantum Electronics*, Vol. QE-23, No. 9, 1462-1476, 1985.

17. C. Warde, A. M. Weiss, A. D. Fisher, J. L. Thackara, "Optical Information Processing Characteristics of the Microchannel Spatial Light Modulator," *Applied Optics*, Vol. 20, No. 12, 2066-2074, 1981.

Table 1. The Relationship Between $S_1(n_1, n_2)$, $S_0(n_1, n_2)$ and $S(n_1, n_2)$.

n_1	n_2	$S_1(n_1,n_2)$	$S_1(N_1-n_1,n_2)$	$S_0(n_1,n_2)$	$S_0(N_1-n_1,n_2)$
0	$0,N_2/2$	$S(0,0)$	$S(0,0)$	0	0
$N_1/2$	$0,N_2/2$	$S(n_1,n_2)$	$S(n_1,n_2)$	0	0
0	$0<n_2<N_2/2$	$S(0,n_2)$	$S(0,n_2)$	$S(0,N_2-n_2)$	$S(0,N_2-n_2)$
$N_1/2$	$0<n_2<N_2/2$	$S(N_1/2,n_2)$	$S(N_1/2,n_2)$	$S(N_1/2,N_2-n_2)$	$S(N_1/2,N_2-n_2)$
$0<n_1<N_1/2$	0	$S(n_1,0)$	$S(n_1,0)$	$S(N_1-n_1,0)$	$-S(N_1-n_1,0)$
$0<n_1<N_1/2$	$N_2/2$	$S(N_1,N_2/2)$	$S(n_1,N_2/2)$	$S(N_1-n_1,N_2/2)$	$-S(N_1-n_1,N_2/2)$
$0<n_1<N_1/2$	$0<n_2<N_2/2$	$S(n_1,n_2)-S(N_1-n_1,N_2-n_2)$	$S(n_1,n_2)+S(N_1-n_1,N_2-n_2)$	$S(n_1,N_2-n_2)+S(N_1-n_1,n_2)$	$S(n_1N_2-n_2)-S(N_1-n_1,n_2)$

Table 2. The 2-D RDFT Amplitudes.

n_1	n_2	$R^2(n_1,n_2)$
0	0	$S^2(0,0)$
$N_1/2$	$N_2/2$	$S^2(n_1,n_2)$
0	$0<n_2<N_2/2$	$S^2(0,n_2)+S^2(0,N_2-n_2)$
$N_1/2$	$0<n_2<N_2/2$	$S^2(N_1/2,n_2)+S^2(N_1/2,N_2-n_2)$
$0<n_1<N_1/2$	0	$S^2(n_1,0)+S^2(N_1-n_1,0)$
$0<n_1<N_1/2$	$N_2/2$	$S^2(n_1,N_2/2)+S^2(N_1-n_1/N_2/2)$
$0<n_1<N_1/2$	$0<n_2<N_2/2$	$S^2(n_1,n_2)+S^2(N_1-n_1,N_2-n_2)$ $+S^2(n_1,N_2-n_2)+S^2(N_1-n_1,n_2)$

Table 3. Classification with the CMF System.

Tool Number	No.1	No.2	No.3	No.4	No.5	No.6	No.7	No.8
No.1	1.0000	0.97610	0.97965	0.97160	0.96361	0.99113	0.97654	0.99111
No.2	1.0000	0.98097	0.98241	0.97460	0.96612	0.99231	0.97934	0.99320
No.3	1.0000	0.97886	0.98298	0.97360	0.96607	0.99221	0.97895	0.99299
No.4	1.0000	0.97913	0.98166	0.97677	0.96574	0.99164	0.97864	0.99208
No.5	1.0000	0.97865	0.98214	0.97374	0.96910	0.99238	0.98102	0.99268
No.6	1.0000	0.97727	0.98072	0.97210	0.96483	0.99283	0.97777	0.99286
No.7	1.0000	0.97891	0.98207	0.97369	0.96804	0.99238	0.98154	0.99279
No.8	1.0000	0.97816	0.98151	0.97255	0.96514	0.99288	0.97820	0.99395

Table 4. Classification with the SBF System.

Tool Number	No.1	No.2	No.3	No.4	No.5	No.6	No.7	No.8
No.1	1.00000	0.25954	0.26660	0.26458	0.27214	0.38480	0.22394	0.34123
No.2	0.25954	1.00000	0.39639	0.27884	0.26760	0.28446	0.33868	0.26397
No.3	0.26662	0.39643	1.00000	0.28699	0.29358	0.30710	0.34722	0.28611
No.4	0.26459	0.27885	0.28699	1.00000	0.28469	0.27654	0.28996	0.25437
No.5	0.27214	0.26760	0.29355	0.28467	1.00000	0.28450	0.26289	0.31970
No.6	0.38480	0.28446	0.30707	0.27653	0.28450	1.00000	0.25671	0.38788
No.7	0.22394	0.33868	0.34719	0.28994	0.26289	0.25671	1.00000	0.28540
No.8	0.34123	0.26397	0.28608	0.25436	0.31970	0.38788	0.28540	1.00000

Table 5. Inspection of the Tool No.7 in Terms of the Output Value.

Tool Number	No.1	No.2	No.3	No.4	No.5	No.6	No.7	No.8
No.7 Broken	248349	356038	370329	296586	283256	262712	949853	300918
No.8 Not Broken	237875	359750	368784	307978	279244	272674	1062189	303156

Table 6. Comparative Performance for the CMF and the SBF as a Function of SNR_1' without Modification.

System	Gaussian Noise Standard Deviation						
	10	20	30	40	50	60	70
NMF	197.666	133.667	101.007	81.182	68.036	58.287	50.937
CMF	6.162	6.155	6.148	6.143	6.138	6.133	6.129

Table 7. Comparative Performance of the CMF and the SBF as a Function of the Modified SNR_1'.

System	Gaussian Noise Standard Deviation						
	10	20	30	40	50	60	70
NMF	197.668	133.671	101.008	81.182	68.036	58.287	50.938
CMF	4.085	4.081	4.076	4.073	4.070	4.067	4.065

Table 8. The Average Distance of the Correlation Peak from the Center of the Correlation Plane with the CFM System (Rectangular Window).

Window Size	Gaussian Noise Standard Deviation						
	10	20	30	40	50	60	70
64	0.000	0.000	0.000	0.000	0.000	0.000	0.000
32	72.000	72.000	71.250	71.000	71.000	54.250	54.250
20	87.250	87.000	87.500	87.500	70.250	71.500	71.500
18	86.250	86.000	86.000	86.000	86.000	111.250	111.000
16	81.250	81.250	81.250	81.250	81.250	81.250	79.750
14	81.250	81.250	81.250	81.250	81.250	81.250	81.250
12	81.250	81.500	81.750	81.750	82.500	82.500	82.500
10	81.000	81.500	81.500	82.250	83.250	83.500	83.500
8	63.250	63.500	63.500	64.000	64.000	90.250	90.250
6	80.500	82.500	83.500	83.500	83.500	83.500	83.500
4	82.000	84.250	86.000	86.000	87.500	87.500	87.500
2	84.250	83.750	88.250	88.250	89.500	89.500	72.500

Table 9. The Average Distance of the Correlation Peak from the Center of the Correlation Plane with the SBF System (Rectangular Window).

Window Size	Gaussian Noise Standard Deviation						
	10	20	30	40	50	60	70
64	0.000	0.000	0.000	0.000	0.000	0.000	0.000
32	0.000	0.000	0.000	0.000	0.000	0.000	0.000
20	0.000	0.000	0.000	0.000	0.000	0.000	0.000
18	0.000	0.000	0.000	10.500	26.250	34.750	34.750
16	0.000	0.000	0.000	0.000	24.750	44.250	60.250
14	0.000	0.000	0.000	42.750	80.250	80.250	70.000
12	0.000	25.000	25.000	80.500	76.000	73.250	64.750
10	24.250	39.250	39.250	42.250	56.000	56.000	54.750
8	23.500	47.250	29.250	62.000	62.000	65.000	65.000
6	66.500	73.000	52.750	57.500	34.250	61.250	62.000
4	81.500	73.000	64.000	69.000	69.000	69.000	69.000
2	78.500	73.750	86.250	65.500	75.500	68.000	75.000

Table 10. The Average Modified SNR_1' with the CMF System (Rectangular Window).

Window Size	Gaussian Noise Standard Deviation						
	10	20	30	40	50	60	70
64	17.141	4.286	4.286	4.287	4.286	4.287	4.288
32	16.290	4.072	4.076	4.081	4.085	4.086	4.076
20	4.073	4.069	4.065	4.056	4.054	4.050	4.045
18	4.075	4.066	4.062	4.062	4.068	4.072	4.079
16	4.097	4.095	4.098	4.103	4.112	4.126	4.139
14	4.215	4.221	4.231	4.241	4.250	4.258	4.269
12	4.364	4.371	4.379	4.390	4.399	4.412	4.427
10	4.543	4.537	4.539	4.556	4.577	4.608	4.640
8	4.563	4.585	4.612	4.649	4.686	4.728	4.773
6	4.920	4.977	5.048	5.121	5.194	5.267	5.336
4	5.153	5.241	5.358	5.486	5.621	5.761	5.888
2	5.418	5.573	5.770	5.962	6.144	6.307	6.446

Table 11. The Average Modified SNR_1' with the SBF System (Rectangular Window).

Window Size	Gaussian Noise Standard Deviation						
	10	20	30	40	50	60	70
64	261.633	50.716	40.320	33.268	28.420	24.647	21.601
32	117.500	22.859	18.305	15.353	13.132	11.303	10.080
20	19.621	15.254	12.440	10.370	8.797	7.489	6.670
18	16.656	12.642	10.053	8.435	7.649	7.256	7.009
16	14.538	11.528	9.800	8.107	7.184	6.947	7.014
14	12.321	10.056	8.532	7.636	7.254	6.924	6.857
12	9.725	8.086	6.891	6.369	6.263	6.359	6.488
10	9.508	8.342	8.061	7.083	7.294	7.059	6.757
8	10.558	8.590	7.707	7.339	7.075	6.715	6.514
6	8.713	7.600	7.175	6.860	6.650	6.570	6.681
4	7.734	7.176	7.225	7.014	6.955	6.879	6.831
2	7.779	6.986	6.917	6.767	6.762	6.652	6.618

Table 12. The Average Distance of the Correlation Peak from the Center of the Correlation Plane with the CMF System (Hanning Window).

Window Size	Gaussian Noise Standard Deviation						
	10	20	30	40	50	60	70
20	55.250	55.250	55.250	54.750	54.750	80.250	80.250
18	79.250	79.250	77.250	77.000	77.000	56.500	56.500
16	79.250	79.250	79.250	79.250	79.250	79.250	78.750
14	78.750	78.500	78.500	78.500	78.500	78.750	78.750
12	78.500	78.500	78.750	80.000	80.500	80.500	80.500
10	78.000	78.250	78.750	80.000	80.250	80.250	80.250
8	61.250	61.750	63.250	64.500	64.250	64.250	64.250
6	77.750	81.750	82.000	82.000	82.000	82.000	82.000
4	82.000	85.500	85.750	85.750	85.750	85.750	85.750
2	81.750	81.250	86.500	86.500	87.750	87.750	70.750

Table 13. The Average Distance of the Correlation Peak from the Center of the Correlation Plane with the SBF System (Hanning Window).

Window Size	Gaussian Noise Standard Deviation						
	10	20	30	40	50	60	70
20	0.000	0.000	0.000	2.750	2.750	2.750	26.250
18	0.000	0.000	0.000	29.750	29.750	45.500	37.000
16	0.000	27.250	23.250	24.750	23.250	53.500	49.250
14	23.000	0.000	0.000	26.500	60.000	59.750	64.500
12	22.750	26.750	54.250	38.000	38.000	38.000	38.500
10	17.750	25.750	65.250	63.750	54.000	63.000	75.000
8	28.500	46.250	46.250	52.250	21.000	34.500	21.000
6	73.000	53.000	53.000	68.750	72.000	96.000	96.000
4	103.750	104.000	88.750	77.750	77.750	71.000	71.750
2	75.000	74.250	107.500	86.750	91.750	84.250	91.250

Table 14. The Average Modified SNR_1' with the CMF System (Hanning Window).

Window Size	Gaussian Noise Standard Deviation						
	10	20	30	40	50	60	70
20	4.073	4.069	4.069	4.068	4.067	4.070	4.073
18	4.089	4.090	4.092	4.095	4.101	4.106	4.116
16	4.173	4.175	4.178	4.182	4.188	4.196	4.206
14	4.303	4.310	4.316	4.322	4.328	4.334	4.343
12	4.458	4.456	4.453	4.458	4.468	4.484	4.502
10	4.602	4.600	4.610	4.634	4.660	4.693	4.728
8	4.595	4.608	4.632	4.674	4.718	4.763	4.810
6	4.950	4.997	5.062	5.133	5.198	5.264	5.329
4	5.178	5.260	5.395	5.536	5.682	5.826	5.957
2	5.416	5.571	5.768	5.961	6.142	6.303	6.443

Table 15. The Average Modified SNR_1' with the SBF System (Hanning Window).

Window Size	Gaussian Noise Standard Deviation						
	10	20	30	40	50	60	70
20	17.617	13.576	11.138	9.365	8.335	7.513	7.225
18	15.736	11.723	9.565	8.158	7.578	7.062	6.760
16	13.417	10.677	9.322	8.132	7.518	7.150	6.946
14	11.466	9.322	8.055	7.054	6.868	6.409	6.432
12	10.515	8.841	7.908	7.136	6.920	6.507	6.271
10	9.257	7.861	7.153	6.423	6.437	6.216	6.120
8	11.093	9.222	8.494	7.843	7.577	7.046	6.876
6	7.917	7.045	7.025	6.993	7.147	6.722	6.732
4	7.253	6.538	6.483	6.546	6.574	6.323	6.376
2	7.451	7.156	6.951	6.996	6.847	6.636	6.549

Table 16. Comparison of the Distances the Actual Window and the Correation Peak has Moved as a Function of Noise Standard Deviation.

Window	Gaussian Noise Standard Deviation							
location	0	10	20	30	40	50	60	70
(0,0)	(0, 0)	(0, 0)	(0, 0)	(0, 0)	(0, 0)	(0, 0)	(0, 0)	(0, 0)
(50,50)	(50, 50)	(50, 50)	(50, 50)	(50, 50)	(50, 50)	(56, 53)	(56, 53)	(56, 53)
(-50,50)	(-50, -50)	(-50, -50)	(-50, -50)	(-50, -50)	(-50, -50)	(-50, -50)	(-50, -50)	(-103, -12)
(50,-45)	(50, -45)	(50, -45)	(50, -45)	(50, -45)	(50, -45)	(50, -45)	(-4, -98)	(-4, -98)
(-45,50)	(-45, 50)	(-45, 50)	(-45, 50)	(-45, 50)	(-45, 50)	(-45, 50)	(-99, -3)	(-99, -3)

Table 17. The Average Distance of the Correlation Peak from the Center of the Correlation Plane with the DSCT1-Based CMF System (Rectangular Window).

Window	Gaussian Noise Standard Deviation						
Size	10	20	30	40	50	60	70
20	2.000	2.000	3.750	3.750	3.750	3.750	4.750
18	2.500	2.500	2.750	4.500	4.500	4.500	4.750
16	2.500	2.500	3.250	3.250	3.250	3.250	3.250
14	3.750	3.750	4.000	2.750	2.750	2.750	4.500
12	6.250	6.250	6.250	6.250	6.250	6.250	5.250
10	10.250	11.500	11.500	10.500	10.500	10.500	10.500
8	6.000	9.000	9.000	12.250	12.250	12.000	12.000
6	8.000	8.250	8.250	11.000	13.500	13.500	13.750
4	23.250	23.250	12.000	15.000	15.000	15.000	13.750
2	20.500	20.500	32.250	32.250	32.250	37.500	34.000

Table 18. The Average Distance of the Correlation Peak from the Center of the Correlation Plane with the DSCT-1 Based SBF System (Rectangular Window).

Window Size	Gaussian Noise Standard Deviation						
	10	20	30	40	50	60	70
20	0.000	0.000	0.000	0.000	14.500	25.250	21.000
18	0.000	0.000	14.000	36.500	44.250	50.250	50.250
16	0.000	0.000	10.500	19.500	26.500	45.250	29.250
14	0.000	0.000	28.750	30.000	30.000	59.750	66.750
12	16.000	23.750	19.750	18.500	14.500	19.000	34.250
10	12.250	14.500	17.000	42.250	43.000	42.250	42.250
8	10.000	20.000	34.250	28.750	45.500	34.000	37.500
6	37.250	33.000	40.000	30.250	57.750	57.500	44.750
4	40.500	45.750	55.500	58.250	49.500	49.500	45.500
2	47.750	33.250	42.500	24.750	52.000	64.750	50.250

Table 19. The Average Modified SNR_1' with the DSCT1-Based CMF Systems (Rectangular Window).

Window Size	Gaussian Noise Standard Deviation						
	10	20	30	40	50	60	70
20	2.205	2.208	2.214	2.221	2.229	2.237	2.248
18	2.243	2.247	2.252	2.259	2.272	2.284	2.297
16	2.264	2.267	2.277	2.288	2.299	2.310	2.321
14	2.281	2.286	2.294	2.304	2.314	2.323	2.336
12	2.293	2.308	2.325	2.344	2.365	2.385	2.408
10	2.381	2.391	2.409	2.433	2.460	2.485	2.513
8	2.446	2.441	2.445	2.457	2.483	2.511	2.538
6	2.646	2.633	2.621	2.623	2.644	2.674	2.702
4	2.764	2.755	2.773	2.810	2.856	2.906	2.954
2	2.939	2.995	3.078	3.151	3.215	3.270	3.343

Table 20. The Average Modified SNR_1' with the DSCT1-Based SBF System (Rectangular Window).

Window Size	Gaussian Noise Standard Deviation						
	10	20	30	40	50	60	70
20	10.119	7.979	6.706	5.681	5.153	4.769	4.519
18	8.293	6.541	5.452	4.630	4.528	4.376	4.135
16	7.627	6.038	5.343	4.745	4.512	4.317	4.245
14	6.408	5.351	4.790	4.485	4.245	4.137	4.118
12	5.122	4.599	4.277	4.200	4.234	4.165	4.091
10	5.321	4.860	4.742	4.208	4.046	3.887	3.891
8	5.996	4.874	4.693	4.421	4.445	4.237	4.144
6	4.679	4.185	4.247	4.067	4.203	4.096	4.062
4	4.194	4.078	3.950	3.970	4.220	4.183	4.146
2	4.211	3.955	3.822	3.924	3.939	3.938	4.097

Table 21. The Performance Coefficients of the CMF and the SBF as a Function of Class Spread Ratio and Window Sizes.

σ^2	ρ	W_x	W_f	ρ^M	ρ^S
0.05	128	$\sqrt{32}$	$\sqrt{32}$	5.86	202.4
0.05	128	4	8	5.86	201.8
0.1	128	$\sqrt{32}$	$\sqrt{32}$	10.74	202.4
0.1	128	4	8	10.74	201.8
1.0	128	$\sqrt{32}$	$\sqrt{32}$	42.95	202.4
1.0	128	4	8	42.95	201.8
2.0	128	$\sqrt{32}$	$\sqrt{32}$	51.54	202.4
2.0	128	4	8	51.54	201.8
3.0	128	$\sqrt{32}$	$\sqrt{32}$	55.22	202.4
3.0	128	4	8	55.22	201.8

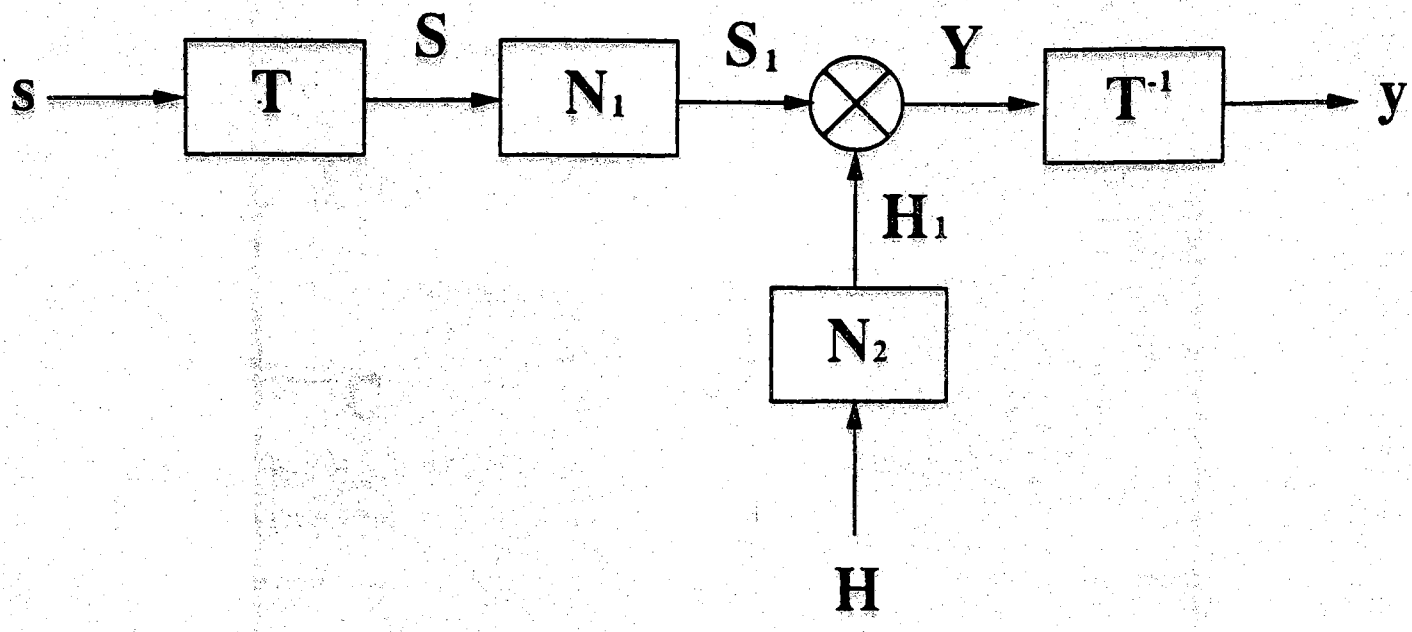

Fig. 1. Block Diagram for Symmetric Nonlinear Matched Filtering.

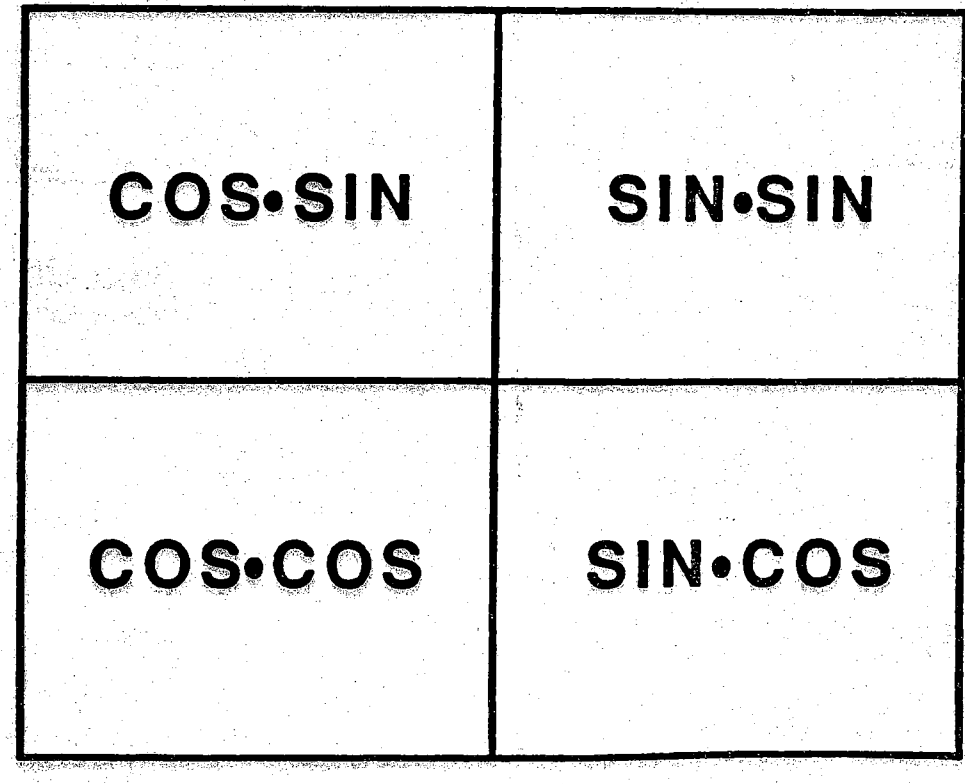

Fig. 2. The Cosine and Sine Operations in the Four Quadrants of the 2-D Real Fourier Transform Spectrum.

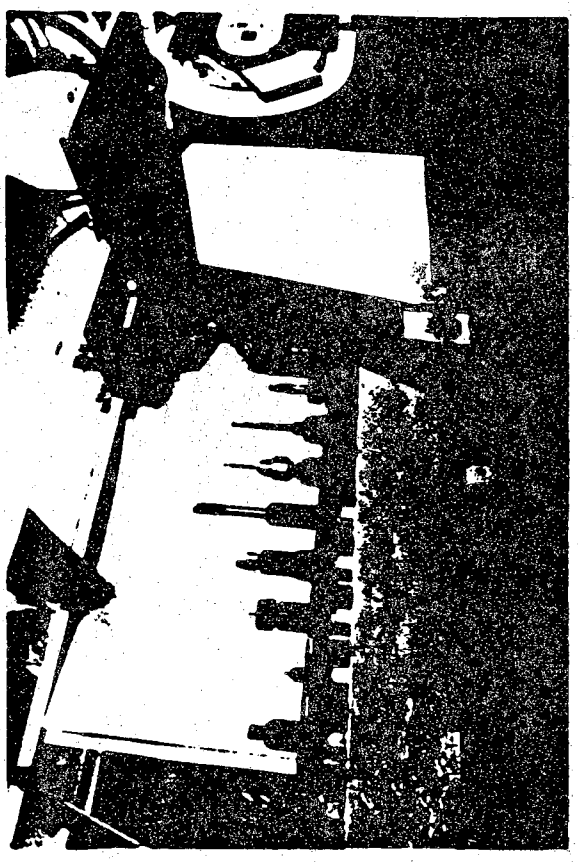

Fig. 3. The Cincinnati Milacron T10 tool chain with camera overhead.

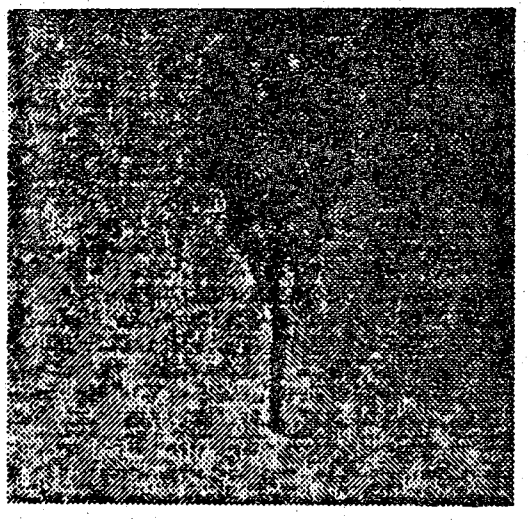

Fig. 4. The Image of the Broken No. 7 Tool.

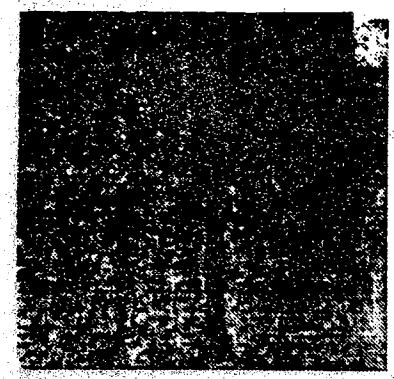

Number 1 Tool

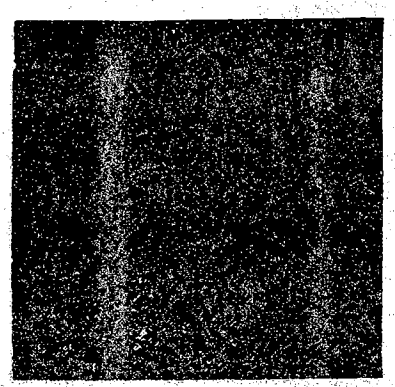

Number 2 Tool

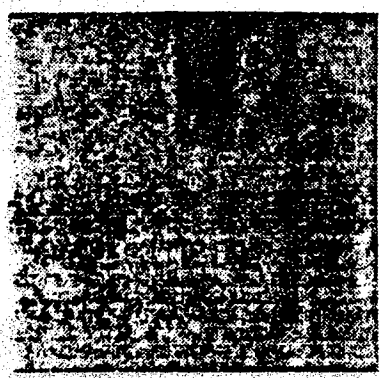

Number 3 Tool

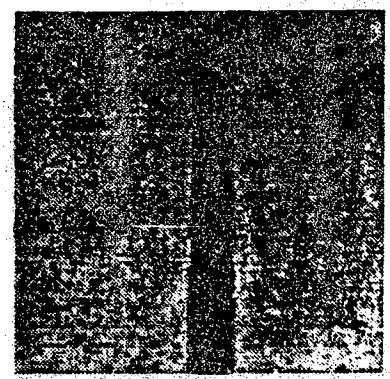

Number 4 Tool

Number 5 Tool

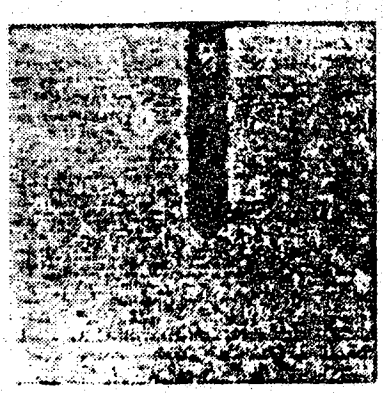

Number 6 Tool

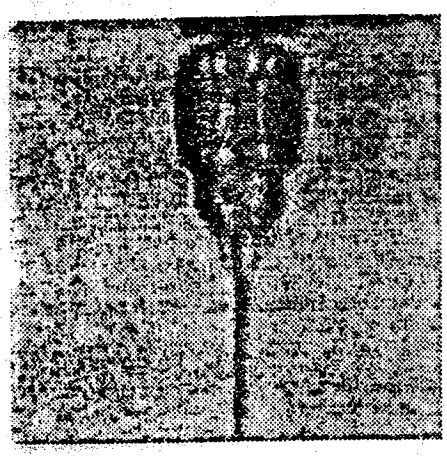

Number 7 Tool

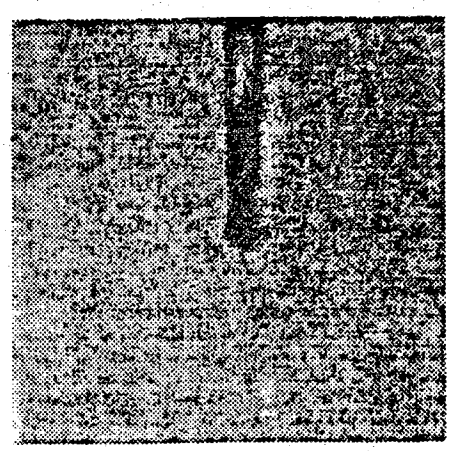

Number 8 Tool

Fig. 5. The Images of the 8 Tools.

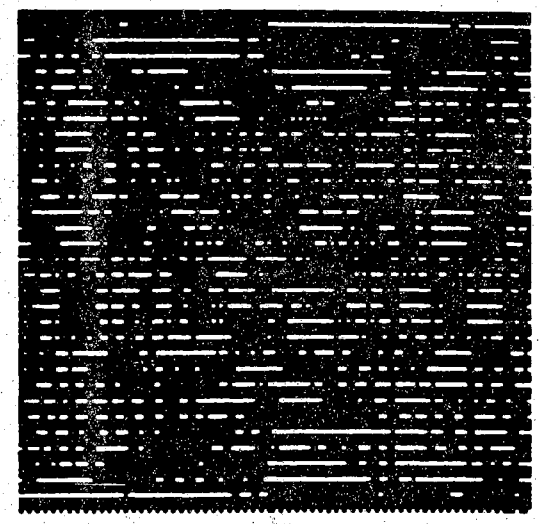

Fig. 6. The Binary Image Obtained by Binarization of the Spectrum of Tool No. 7.

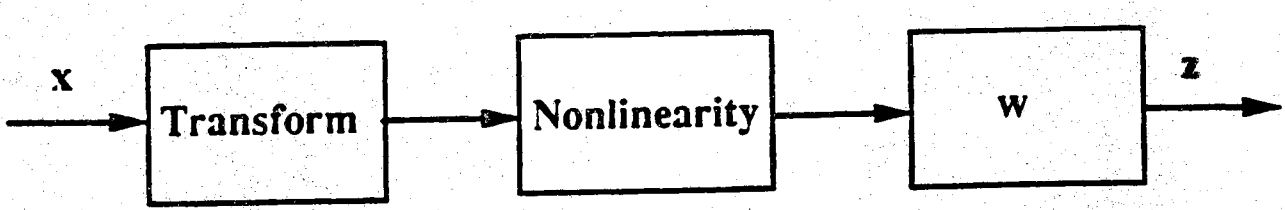

Fig. 7. The Three-Layer Neural Network Interpretation of the Nonlinear Matched Filter.

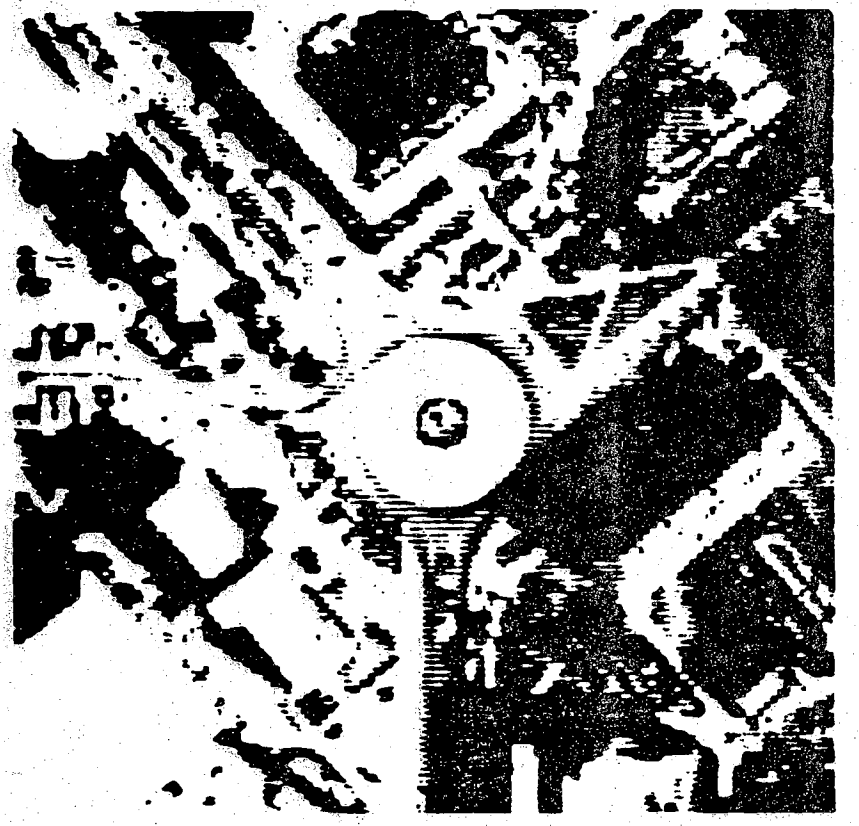

Fig. 8 Purdue Campus Image of Size 128 × 128.

Fig. 9. Purdue Image Corrupted by White Gaussian Noise of Standard [illegible]

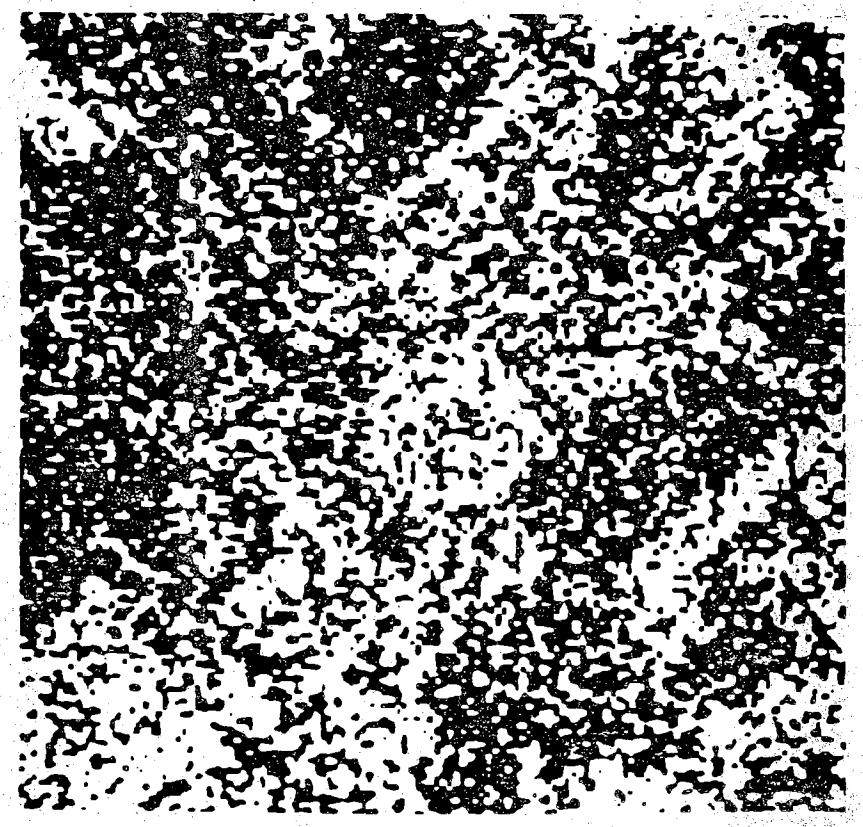

Fig. 10. Purdue Image Corrupted by White Gaussian Noise of Standard Deviation [illegible]

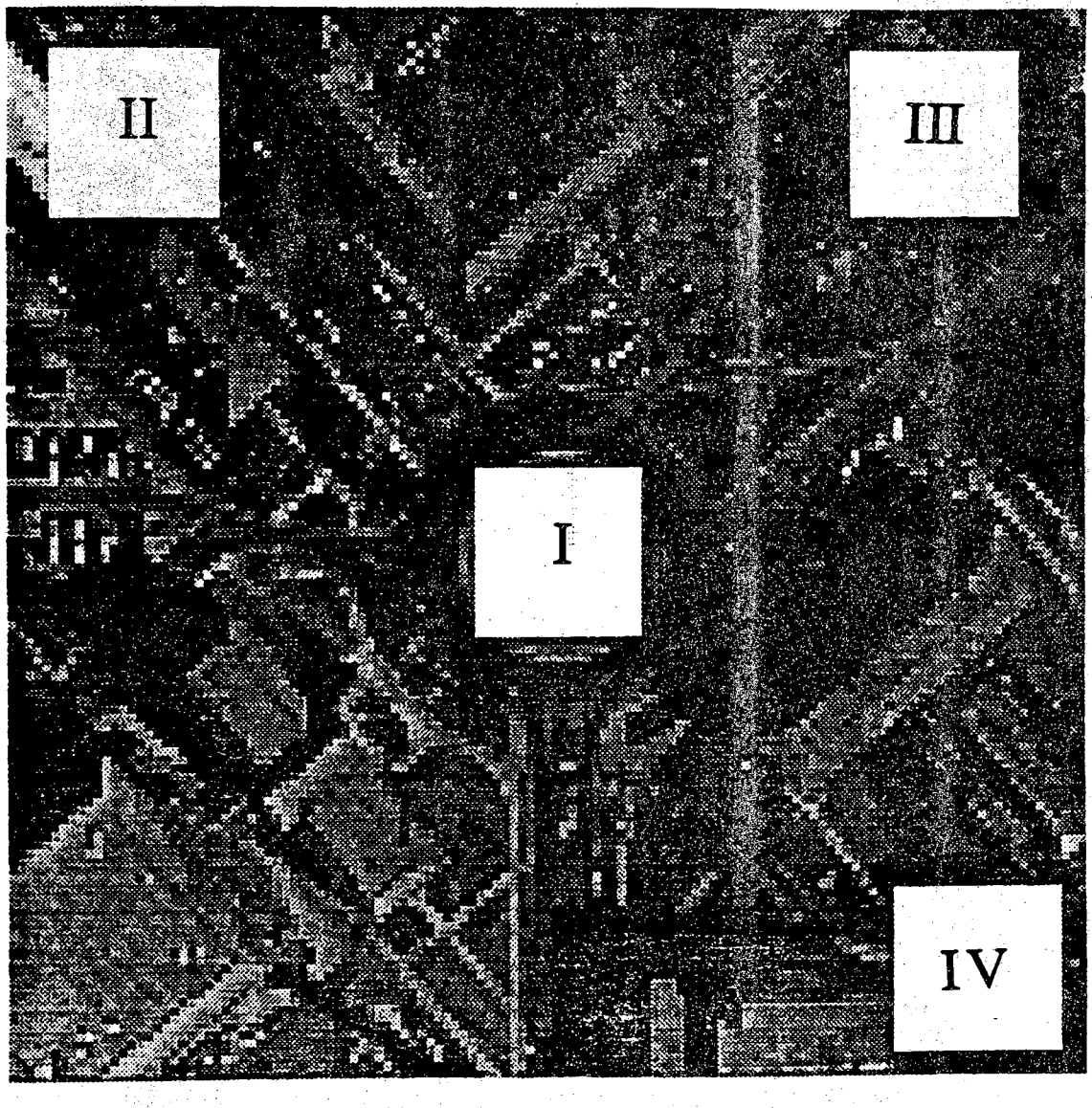

Fig. 11. Four Different Window of Size 20 × 20 in the Purdue Image.

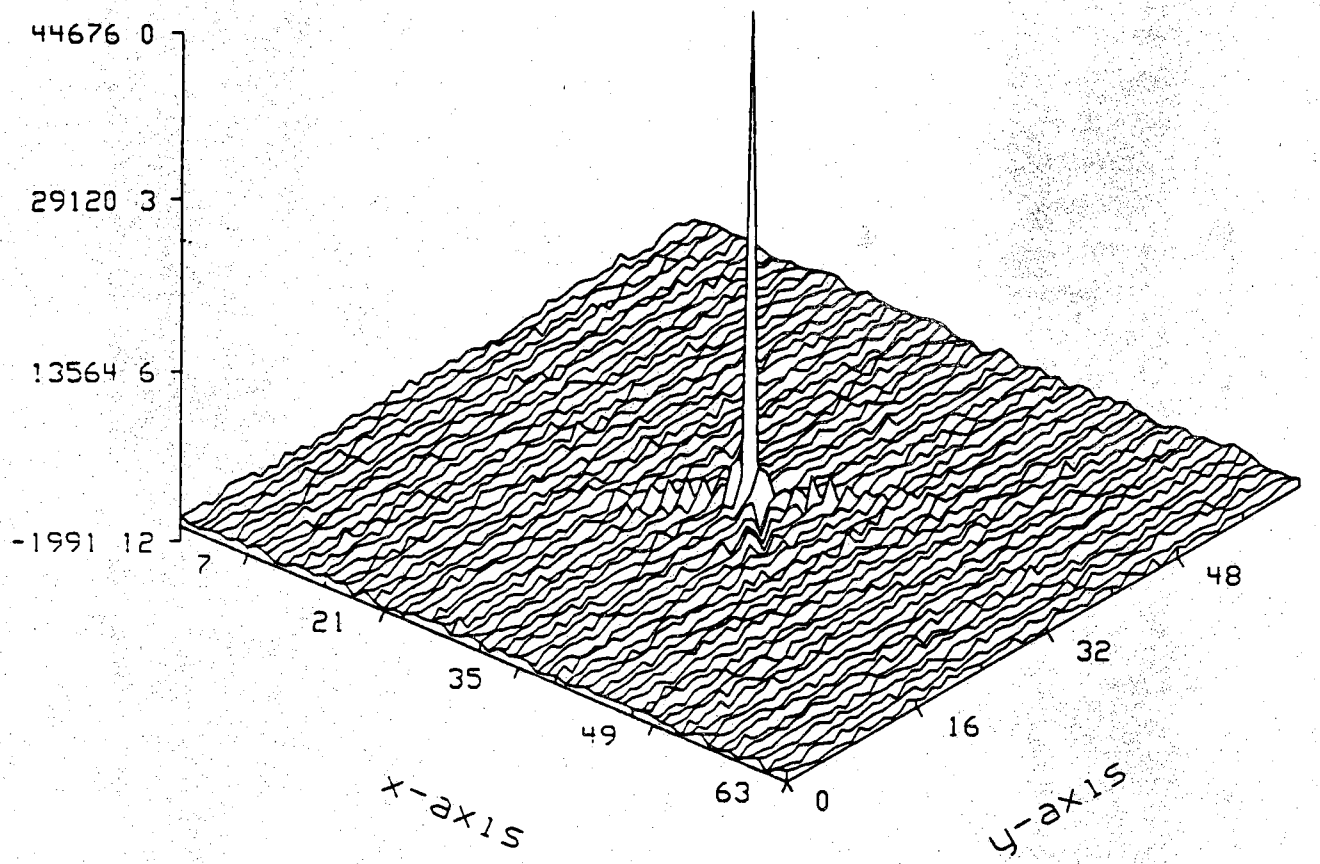

Fig. 12. The Output of the RDFT-Based SBF when the Purdue Image is Correlated with itself.

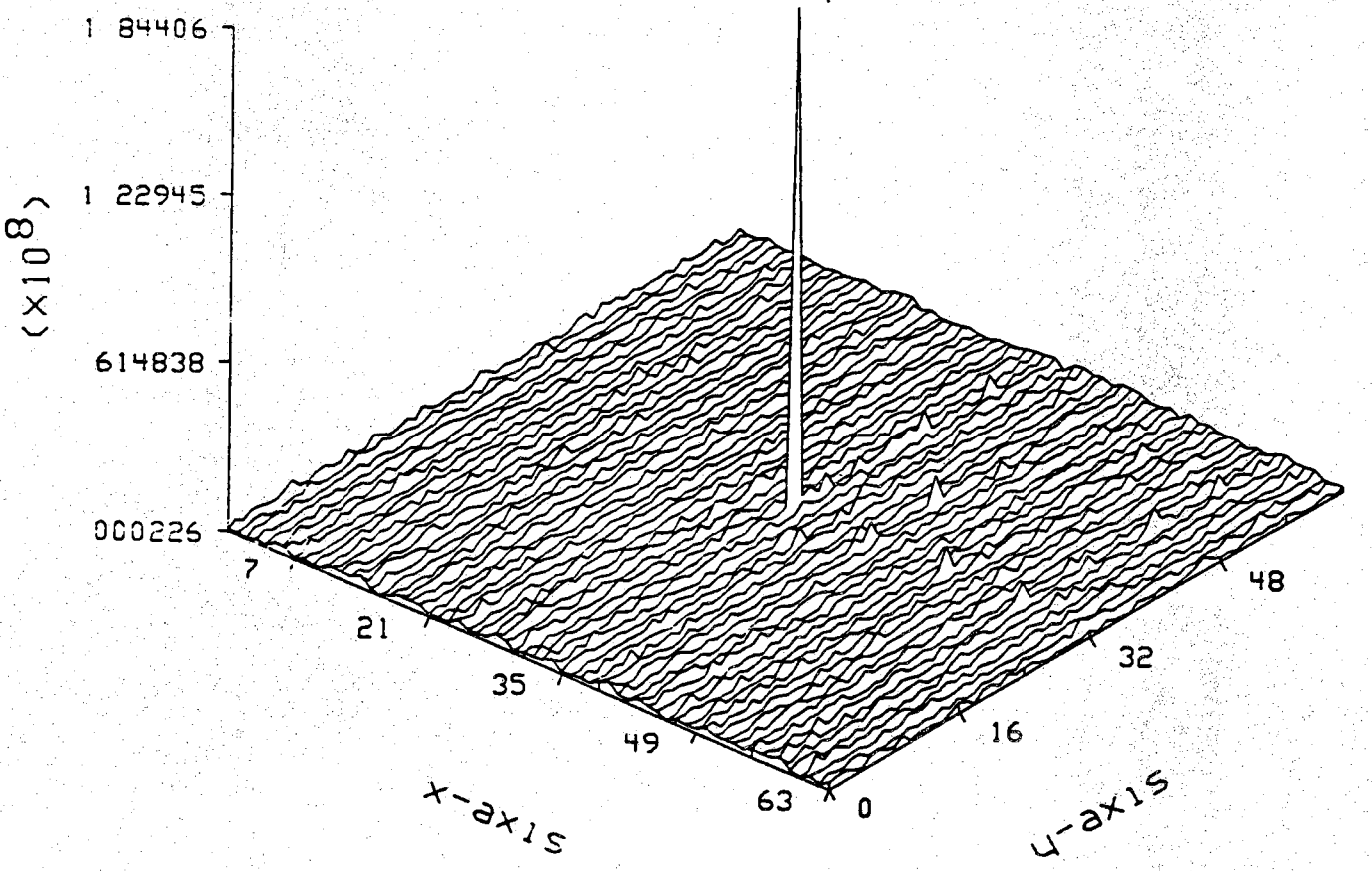

Fig. 13. The Output of the DFT-Based SBF when the Purdue Image is Correlated with itself.

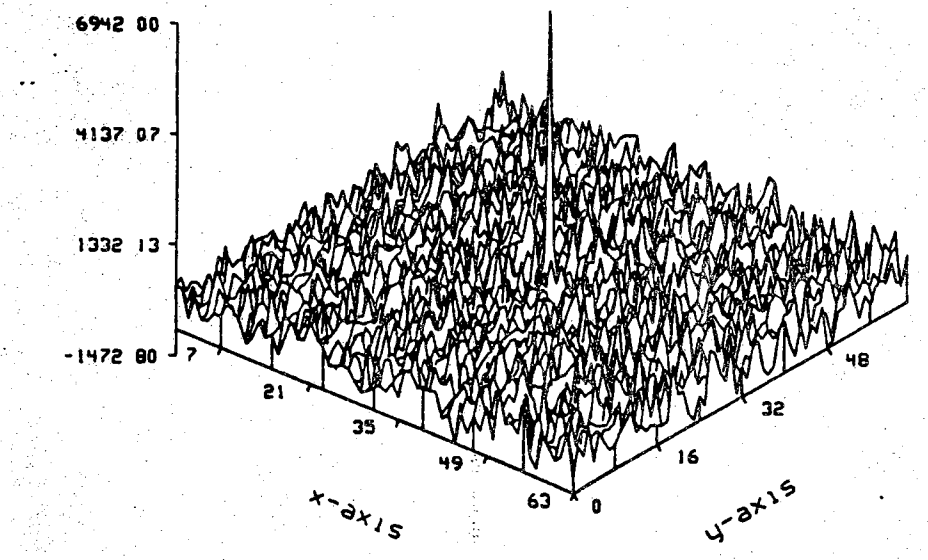

Fig. 14. The Output of the RDFT-Based SBF when the Purdue Image is Correlated with its Central 32 × 32 Block.

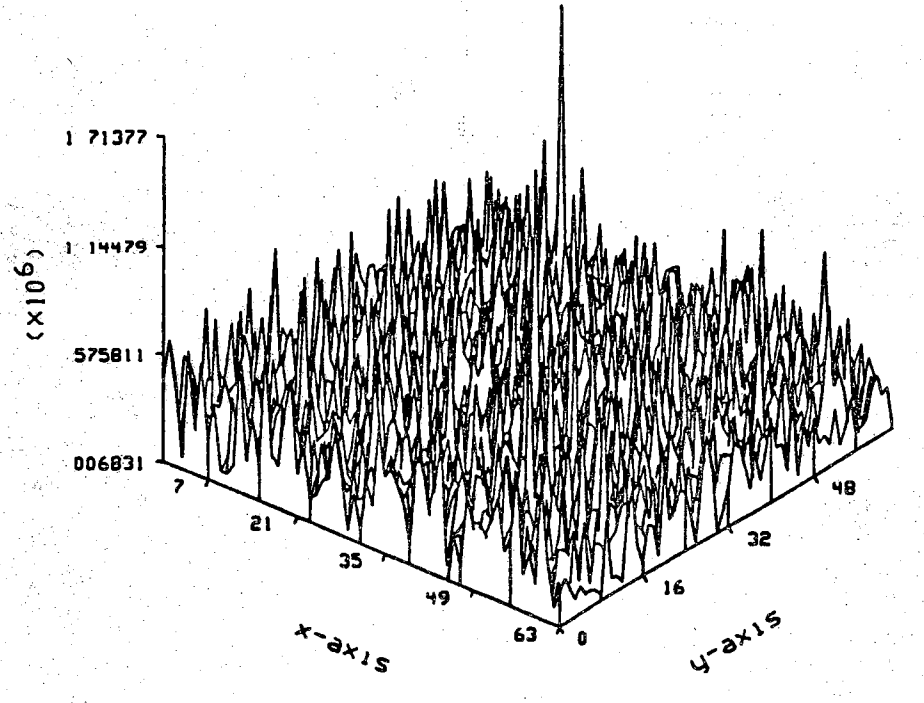

Fig. 15. The Output of the DFT-Based SBF when the Purdue Image is Correlated with its Central 32 × 32 Block.

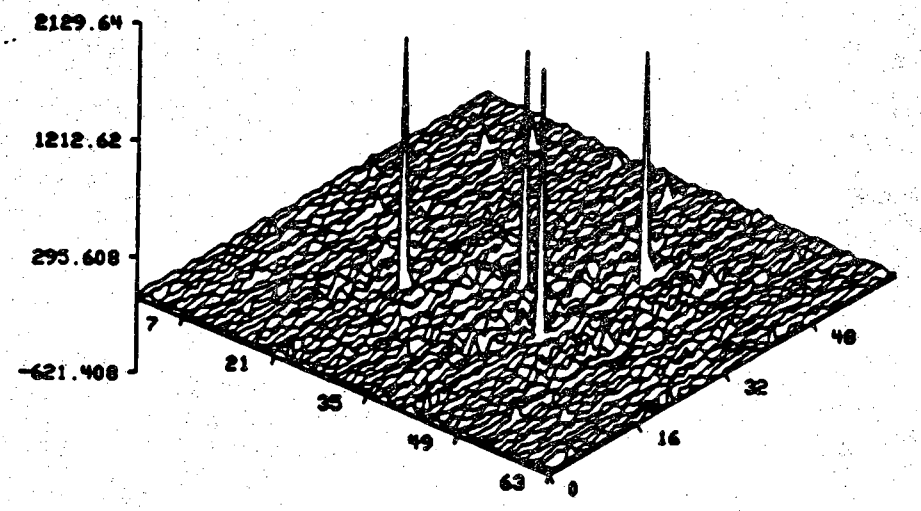

Fig. 16. The Output of the RDFT-Based when the Letter E Repeated Four Times is Detected.

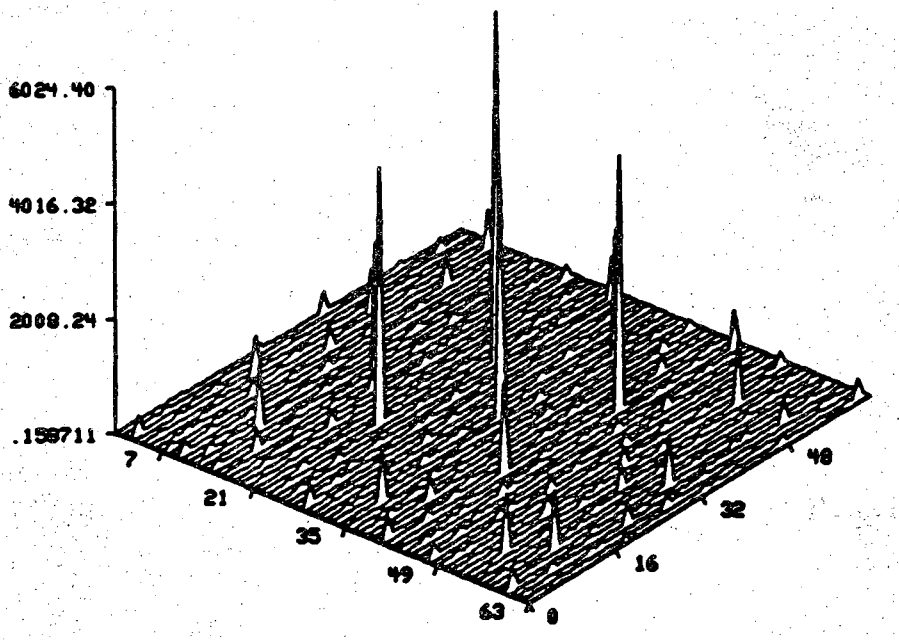

Fig. 17. The Output of the DFT-Based SPOF when the Letter E Repeated Four Times is Detected.

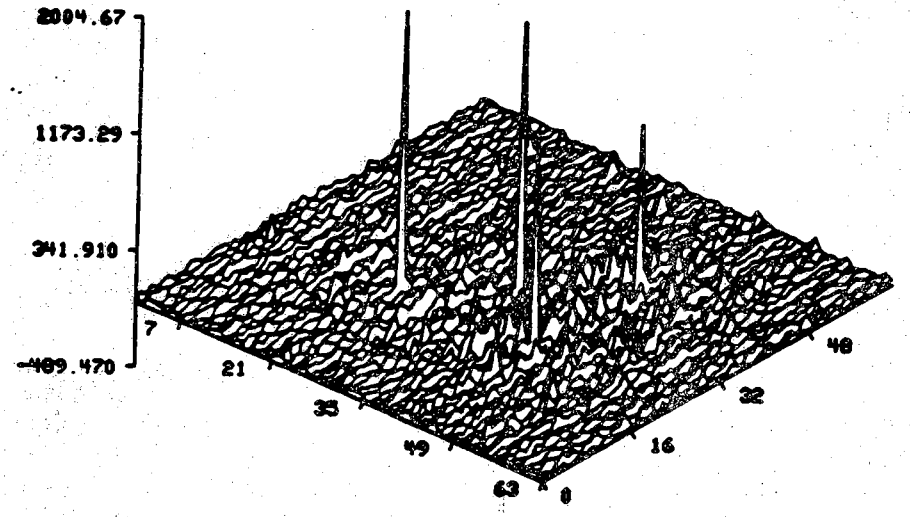

Fig. 18. The Output of the RDFT-Based SPOF when 2 E's and 2 F's are Detected with the E Filter.

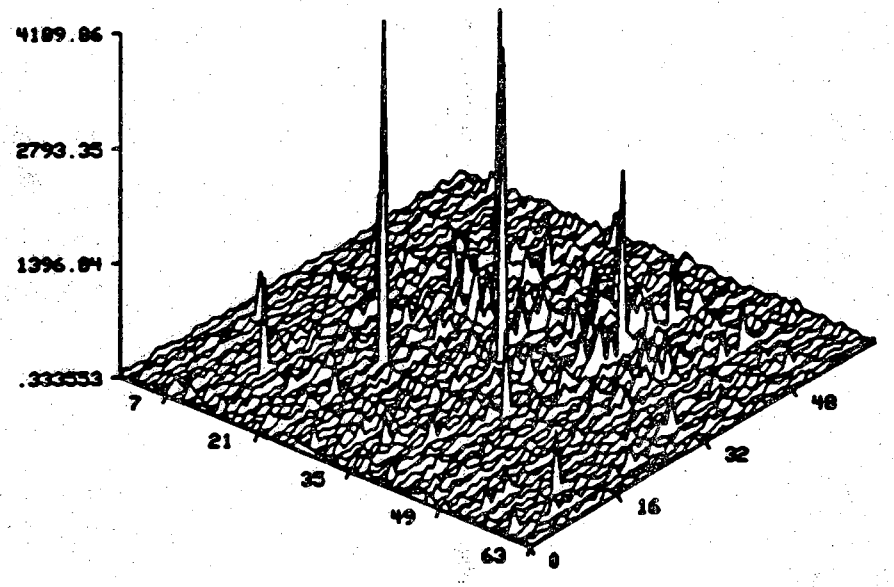

Fig. 19. The Output of the DFT-Based SPOF when 2 E's and 2 F's are Detected with the E Filter.

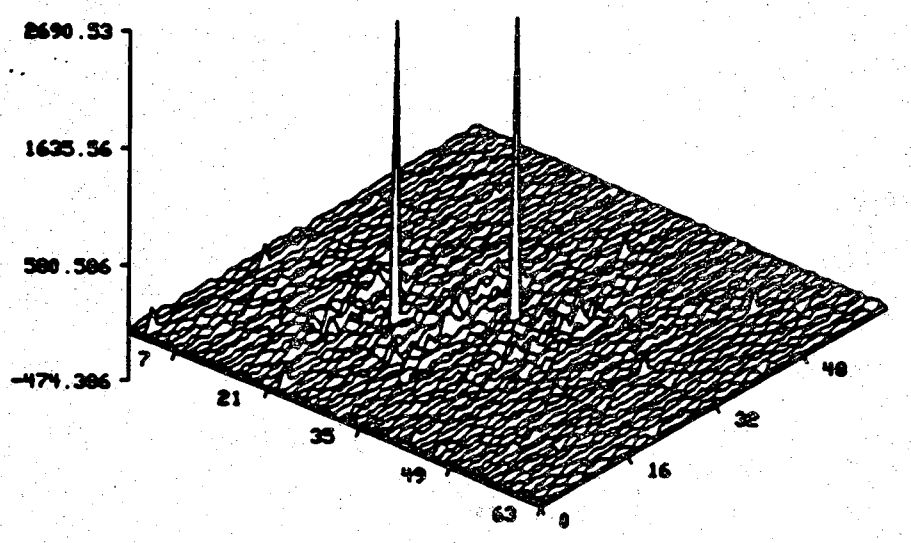

Fig. 20. The Output of the RDFT-Based SPOF when 2 Letter E's are Detected.

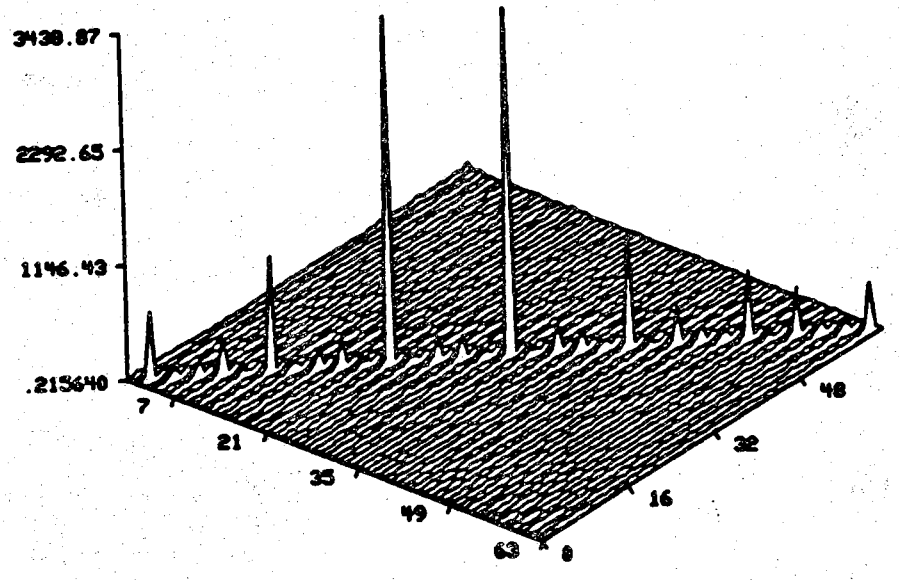

Fig. 21. The Output of the DFT-Based SPOF when 2 Letter E's are Detected.

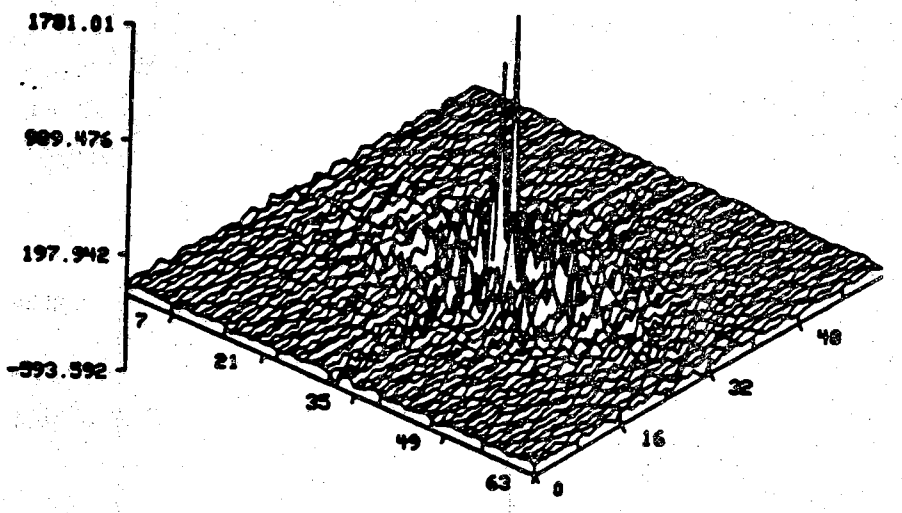

Fig. 22. The Output of the RDFT-Based SPOF when a Letter E and Another Closeby Letter E Partially Hidden and Hidden Part Removed is Detected.

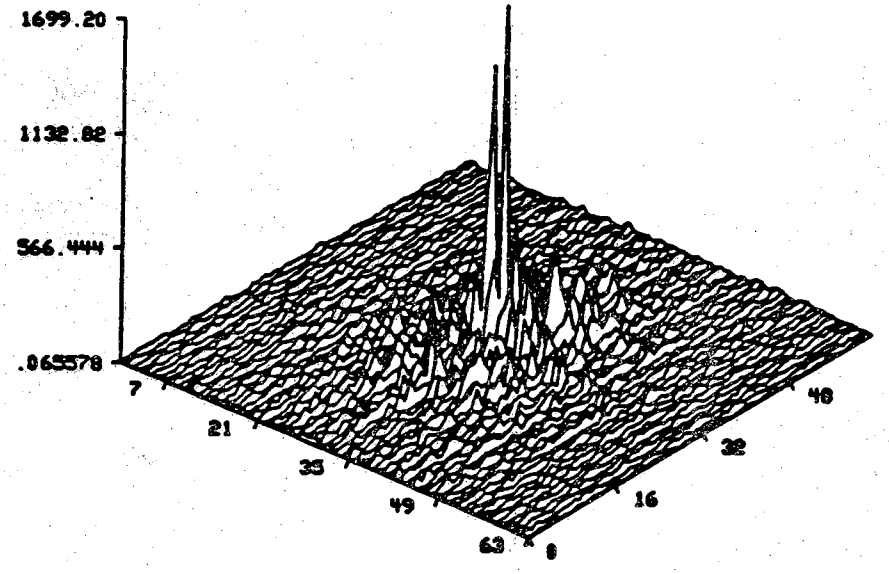

Fig. 23. The Output of the DFT-Based SPOF when a Letter E and Another Closeby Letter E Partially Hidden and Hidden Part Removed is Detected.

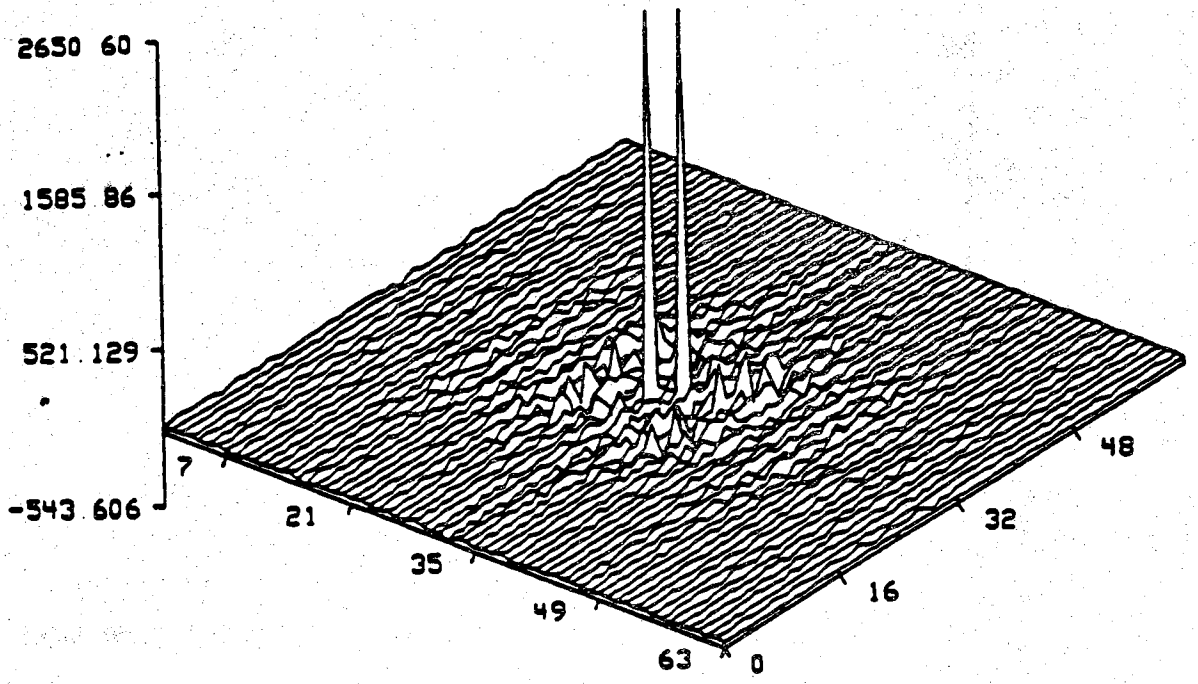

Fig. 24. The Output of the RDFT-Based SPOF when a Letter E and Another Closeby Letter E Added Together is Detected Without Hidden Part Removal.

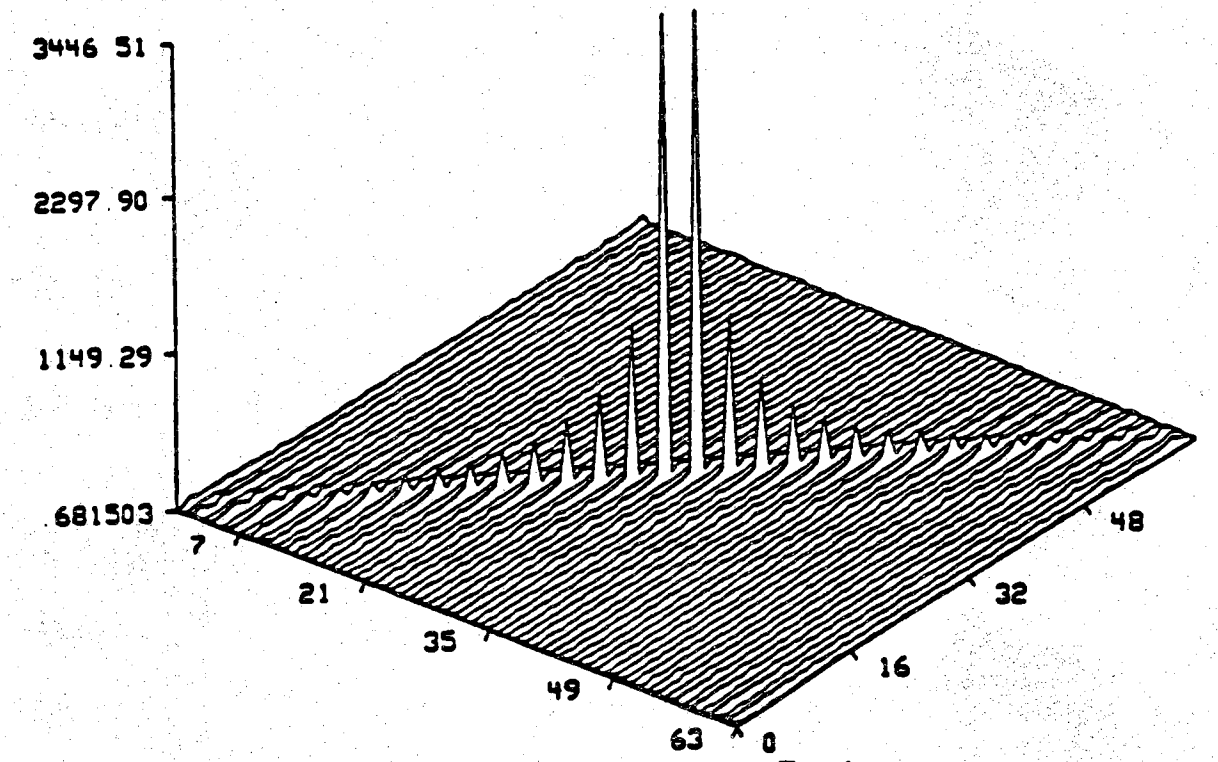

Fig. 25. The Output of the DFT-Based SPOF when a Letter E and Another Closeby Letter E Added Together is Detected Without Hidden Part Removal.

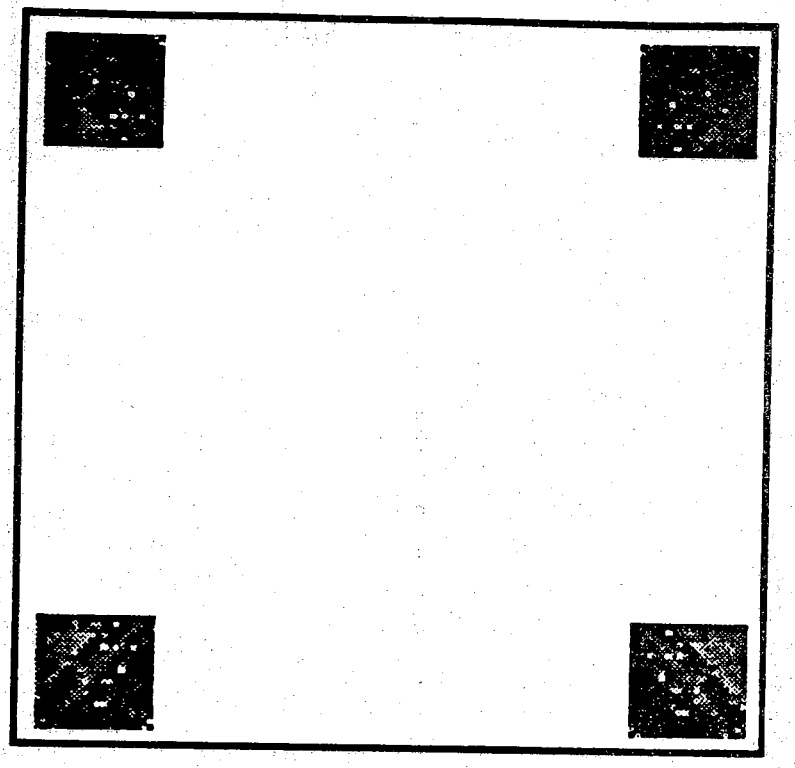

Fig. 26. 4-Fold Symmetric Image.

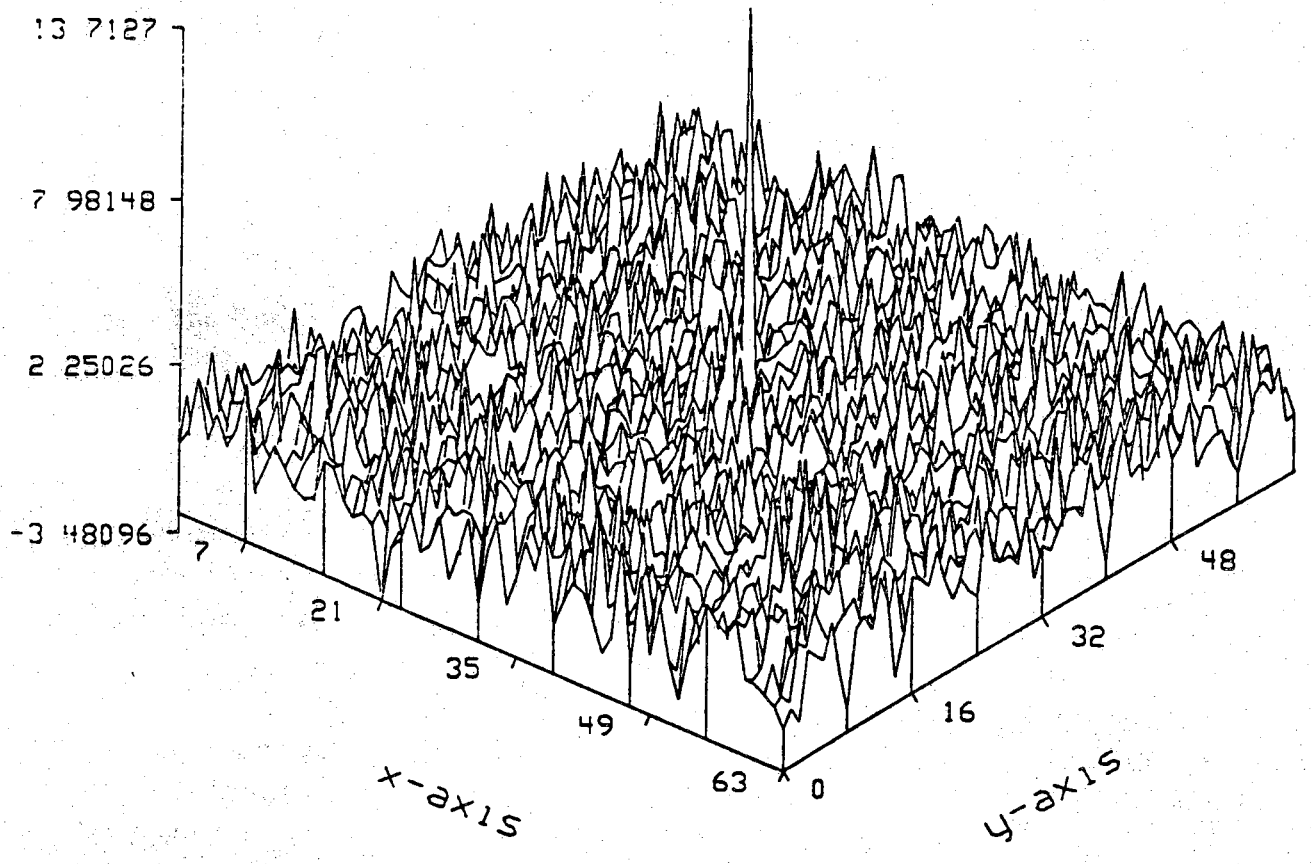

Fig. 27. The Output of the DSCT1-Based SBF when the Purdue Image is Correlated with Itself.

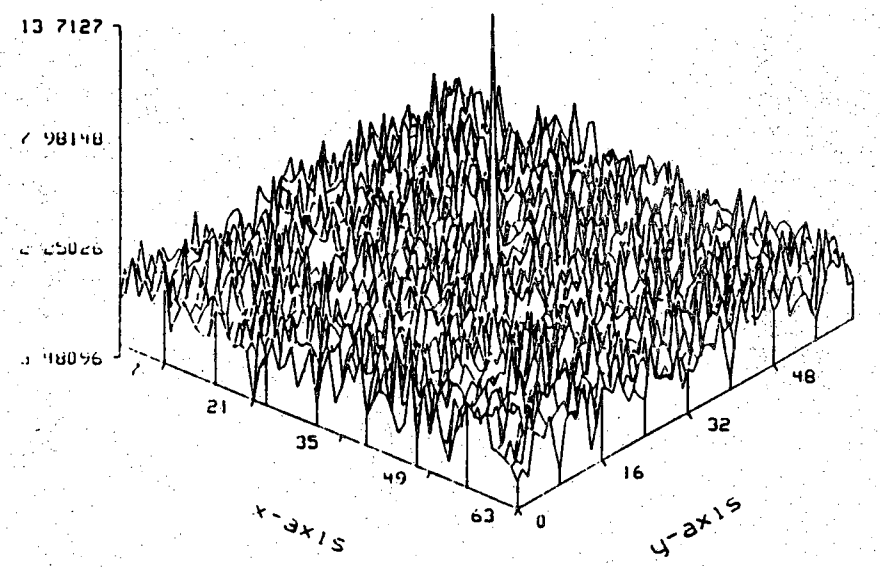

Fig. 28. The Output of the DSCT1-Based SBF when the Purdue Image is Correlated with its Central 32 × 32 Block.

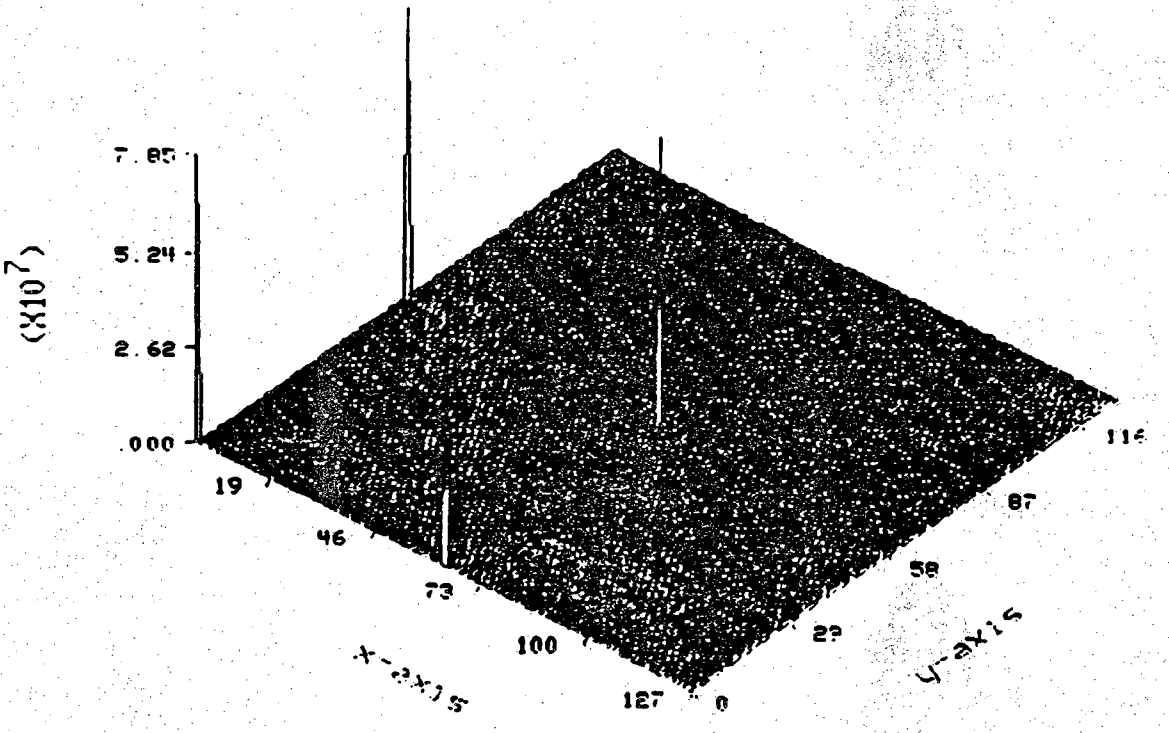

Fig. 29. The Output of the DSCT2-Based SBF.

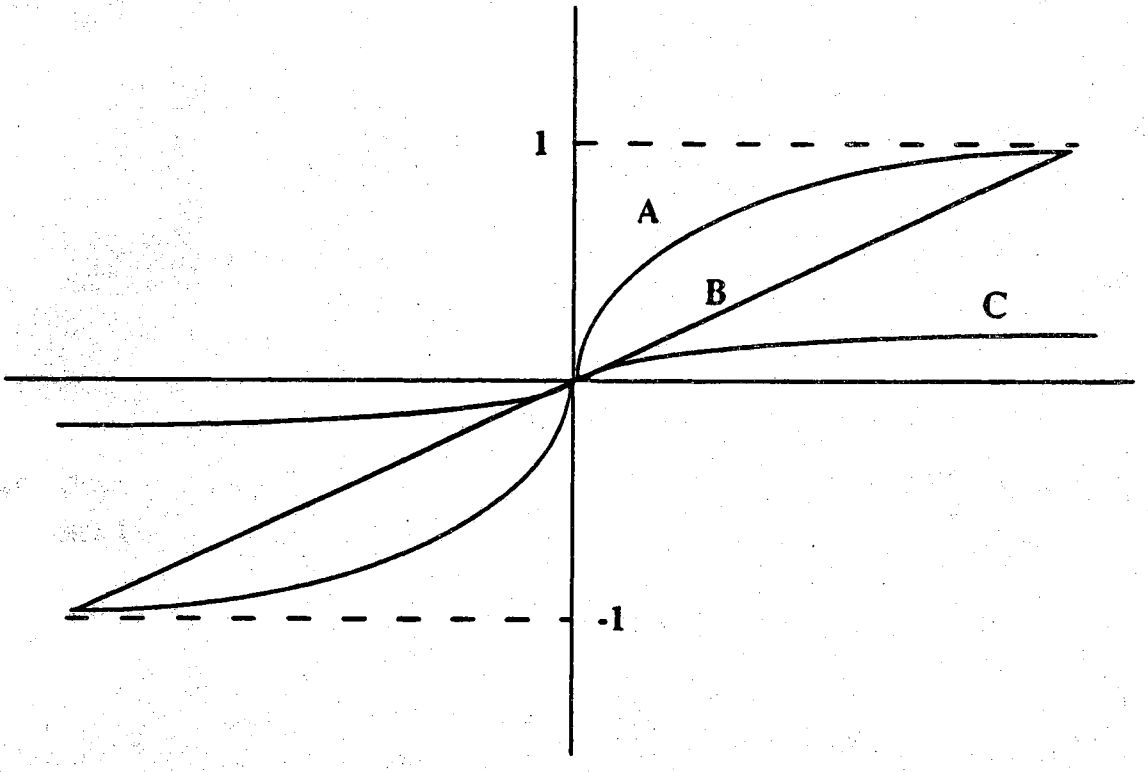

Fig. 30. Three Types of Nonlinearities: A) Stepper than Linear B) Linear C) Less Steep than Linear.